Quantifying the Role of Eddy-Zonal Flow Feedback on Zonal Wind Variability using a Two-Mode Approach

---

Author

Christopher Begalke

A thesis submitted in partial fulfillment of the requirements for the degree of

MASTERS OF SCIENCE

(Atmospheric and Oceanic Sciences)

at the

UNIVERSITY OF WISCONSIN-MADISON

2018

Thesis Declaration and Approval

I, Christopher John Begalke, declare that this thesis titled “Quantifying the Role of Eddy-Zonal Flow Feedback on Zonal Wind Variability using a Two-Mode Approach” and the work presented in it are my own.

Christopher Begalke

Author Signature Date

I hereby approve and recommend for acceptance this work in partial fulfillment of the requirements for the degree of Master of Science:

Dr. David Lorenz

Committee Chair Signature Date

Dr. Daniel Vimont

Faculty Member Signature Date

Dr. Jonathan Martin

Faculty Member Signature Date

Abstract

The poleward propagation of zonal-mean zonal wind anomalies is a major but often neglected component of zonal-mean variability. Poleward propagation is essential for understanding the response of the jet streams to global warming, in particular, why does the jet shift poleward in response to greenhouse gas forcing. Traditionally, the study of zonal-mean zonal wind has focused on the annular mode, which is the leading EOF of zonal wind variability outside of the tropics. Focusing on a single EOF, however, ignores the coupling between EOFs that are a prerequisite in the presence of propagation. This narrow uncoupled EOF view has dominated studies quantifying the feedbacks between zonal-mean zonal wind anomalies and the eddy momentum fluxes that force them. This study generalizes the analysis of the eddy-zonal flow feedbacks to multiple coupled EOFs. In the process, we quantify the role of eddy-zonal flow feedbacks on zonal-mean zonal wind variability and persistence in the ERA-Interim reanalysis (1979-2017). We find that the role of feedbacks on zonal-mean zonal wind variability is significantly larger than that found when assuming uncoupled EOFs.

Acknowledgements

There are a handful of individuals that I need to acknowledge because without them, none of this would have been possible. First and foremost, I could not have done any of this without my fantastic research advisor Dr. David Lorenz. He provided topnotch mentorship and support throughout my research project and my entire time in graduate school. I would also like to express my gratitude to my two other committee members, Dr. Daniel Vimont and Dr. Jonathan Martin, for taking the time out of their busy schedules to provide crucial feedback on my research. Special thanks to Dan for his statistics and climatology classes which provided me with many useful tools and techniques used directly in this work.

I would also like to thank the entire AOS staff as they have been instrumental in keeping me on track from day one. The technical and financial support from the department provided me with the necessary resources to complete this research.

I must also mention the fantastic support I have had from friends and family. The support from my fellow graduate students and the many friendships formed will last long past UW. I cannot thank my amazing family enough for their love and support throughout this process. They have always been so encouraging, caring, and understanding while I have tackled this challenging academic journey. And last, but certainly not least, my incredible girlfriend, Nellie, has been with me, encouraging me, and driving me to reach my full potential and driving me to be the best person I can be. There is no way I could have done this without her and for that, I am so thankful to have her by my side.

Table of Contents

List of Figures

List of Tables

List of Equations

1. Introduction

Over the last half century, the study of the effects of eddies on the zonal-mean state of the atmosphere attempts to better understand the jet stream that plays such an integral role in the climate of the planet (Lorenz & Hartmann, 2001) (Lorenz & Hartmann, 2003) (Gerber & Vallis, 2006). The changing climate is becoming a hot-button topic and one that needs constant exploration through rigorous scientific review. While the public awareness of the changing climate is more recent, the concept of studying the variability in the zonal-mean state is not quite as new. In the late 1930's, Rossby began to study how fluctuations in the intensity of the zonal circulation as a whole could lead to the displacement of "atmospheric centers of action", which are understood today as quasi-stationary high and low-pressure centers. One of the key aspects of Rossby's research was the introduction of the zonal index. He defined the terms "high" and "low" zonal-index patterns to correspond to strong and weak mid-latitude westerlies, respectively. In 1948, Willett studied the impact of these zonal-index patterns on the general circulation with respect to both latitudinal and longitudinal shifts in portions of the general circulation (Willett, 1948). In 1950, Namias took the concept of a zonal index and used it to analyze the effect on the general circulation. He found that the mid-latitude westerlies serve as a divider of the cold air in the polar regions and warmer air equatorward. He states that the zonal index cycle defines how strong these westerlies, also known as the jet stream, fluctuate and lead to these cold air outbreaks which are necessary for the atmospheric heat balance (Namias, 1950). Understanding the strength of the jet stream using these zonal indices is a useful tool in understanding and explaining how the general circulation and atmospheric heat balance are intimately tied to the zonal-mean state of the atmosphere. In recent years, the study of the zonal-

mean state in the atmosphere and more specifically, the variability in the zonal-mean state have ramped up.

1.1 Defining annular modes and zonal index

After initial research findings on the zonal-mean state of the atmosphere, further research took on the task of investigating the causes of the variability in the zonal-mean state and the general circulation. The modes of this variability are key in understanding how a variable that varies in regard to strength or location or some other manner. The dominant mode of variability is located near the midlatitude jet (centered around 50°S). This variability explains roughly 40% of the variance of the zonal wind in the Southern Hemisphere when using twice-daily data (Nigam, 1990). The Southern Hemisphere is more commonly studied in past papers due to the more consistent nature of the zonal-mean state structure. Many of these studies can be applied to the Northern Hemisphere, but there are some additional complexities to consider when studying the Northern Hemisphere. For example, stationary eddies are more prevalent in the Northern Hemisphere momentum budget than they are in the Southern Hemisphere (Lorenz & Hartmann, 2001). Also, the Northern Hemisphere contains more longitudinal asymmetries than the Southern Hemisphere (Lorenz & Hartmann, 2003). The focus of this paper will be on the Southern Hemisphere. The robust nature of this mode is shown through its prevalence in all seasons with similar variance in all seasons (Hartmann & Lo, 1998). Earlier, we stated that Rossby identified high and low index patterns by the strength of mid-latitude westerlies, but for this paper, we will refer to high index as the time when the jet is poleward of its mean position and low index when the jet is equatorward of its mean position. The zonal index will refer to the strength of this dominant mode (Lorenz & Hartmann, 2001). The second mode that also

explains a significant amount of variance is a stationary fluctuation in the jet speed and jet width (Nigam, 1990). For example, the positive second mode of zonal-mean zonal wind will show a strengthening and narrowing of the jet while a negative second mode will show a weakening and broadening of the jet. We will attempt to duplicate these results later in this paper. The importance of this finding and understanding of the modes of variability cannot be understated. The dominant mode of variability is the north and south shift of the jet region while the second mode is the relative strengthening or weakening of the jet. We hope to address the feedback between these two dominant modes and eddy momentum flux in this paper.

The dominant mode of zonal mean zonal wind variability that resides between 40°S and 60°S is often referred to as the "Southern Annular Mode". Due to the robust and significant nature of the variability, many people have investigated the annular mode. The pattern of variability can be seen across many different timescales, from daily to monthly means to seasonal (Nigam, 1990). The variability in the leading modes are seen in both hemispheres and show clear similarities, but for this paper, the focus will stay in the Southern Hemisphere. In the Northern hemisphere, the leading mode, or annular mode, is defined as the Arctic Oscillation (AO) index, also referred to as the Northern Annular mode (NAM) (Thompson & Wallace, 2000). In the Southern hemisphere, the leading mode, or annular mode, is defined as the Southern Annular Mode (SAM).

The annular mode was initially defined as the first EOF of the sea level pressure, which was later found to be very similar to the zonal-mean zonal wind (Thompson & Wallace, 2000). We hope to be able to use an understanding of the annular mode to improve the predictability of the changes in the zonal-mean zonal wind. One interesting theory on the annular modes is that climate predictability is high if the dominant form of internal variability represents the zonal

index and the predictability is lower if the dominant form of variability is defined as the poleward propagation (Son & Lee, 2006). However, in practice, these dominant modes of variability will coexist in a single climate state. Predictability will be high if the ratio of fractional variance of EOF2 to EOF1 does not exceed 0.5 (Son & Lee, 2006). Poleward propagation is also important for the poleward shifted jets under climate change because direct radiative effect of increased greenhouse gasses is to increase strength of the jet (Lorenz D. , 2014). The poleward shift under climate change is only achieved through the same sort of eddy feedbacks that cause poleward propagation.

Annular modes can take on a different structure in different climates due to the changes in climatological features, like the latitude of mean jets and the relative strength of baroclinic zones. With the changes in the annular mode structure, the dominant variability could change as well through a change in altitude, variance, or a jet shift seesaw (Codron, 2004). Codron finds that changes in the background state through zonal asymmetries or time do not modify basic SAM, but they could change the local amplitude of SAM by forcing changes or strength of feedback and their local relation between variability and climatological features. The preferred meridional structure will be the one that yields the strongest eddy feedback given the local mean state (Codron, 2004).

1.2 Evidence for a shifting jet

Understanding the jet stream and the potential poleward propagation is something of significant importance moving forward in a changing climate. More recent research is starting to find the jet may be shifting poleward in future climate simulations, but this poleward shift is evident in past climate reanalysis as well (Feldstein S. B., 1998). Feldstein (1998) used reanalysis data to assess the poleward propagation of the zonal mean flow anomalies in both the Northern and Southern Hemisphere. In Fig. 1, we see the results of the analysis of the angular

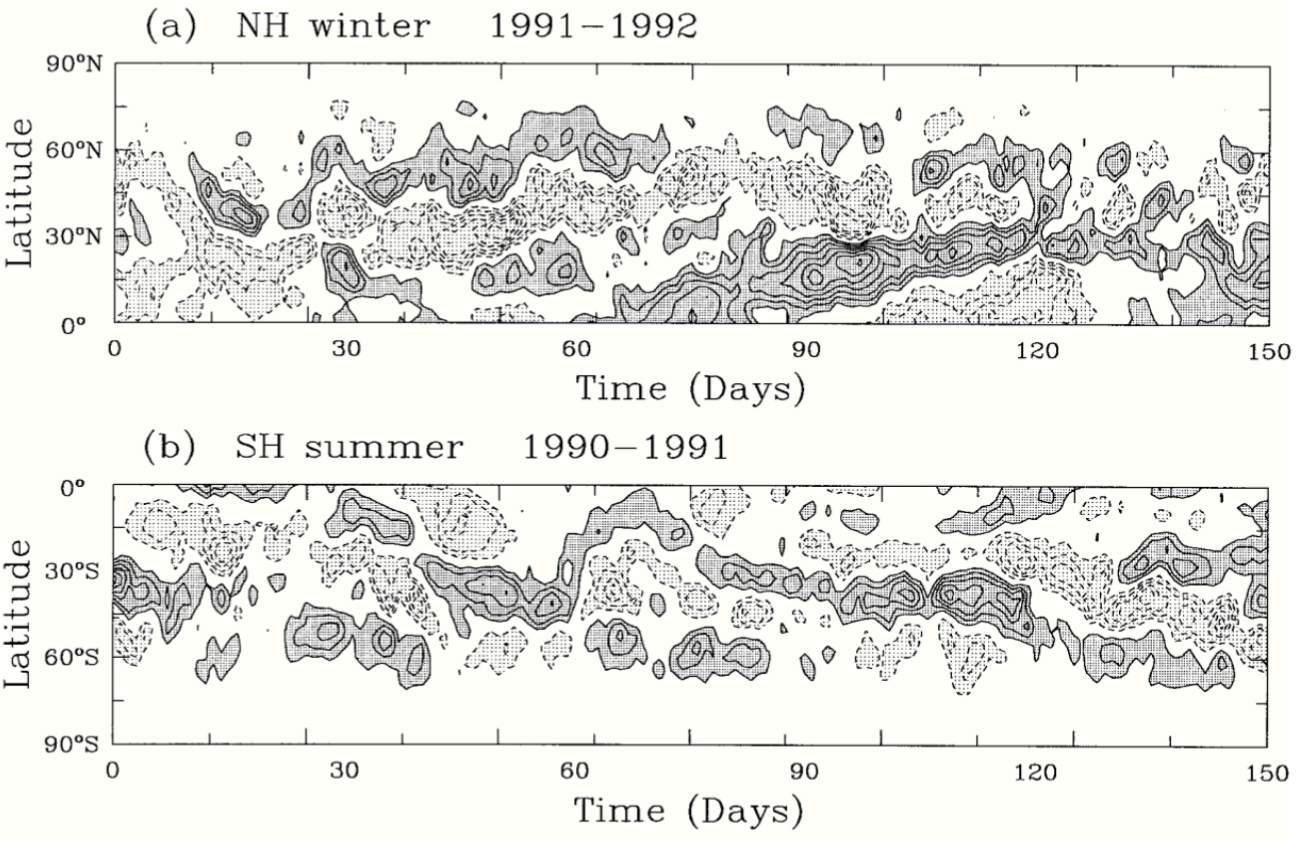

Figure 1. *Fig. 1 from Feldstein (1998) showing the anomalous angular momentum for a) NH Winter 1991-1992 and b) SH Summer 1990-1991. The solid (dashed) contours are positive (negative) anomalies. Dark (light) shading denotes positive (negative) values. The contour interval is* $0.4\ X\ 10^{24} kg\ m^2 s^{-1}$.

momentum anomalies, which is another good proxy to depict the jet stream anomalies, in the NH winter from 1991-1992 and the SH summer from 1990-1991 (Feldstein S. B., 1998). Fig. 1 plots the angular momentum anomalies with respect to time and latitude to capture the potential

propagation of these anomalies. It is quite clear that the anomalies have a significant poleward movement as they propagate through time. For example, in Fig. 1b, at time = 70 days, there are significant positive anomalies at about 10°S. As we follow this positive anomaly, we see it slowly but definitively propagate poleward, eventually reaching about 70°S near time = 130 days. We see similar occurrences throughout both Figs. 1a and 1b which illustrate the tendency for poleward propagation in the zonal mean flow anomalies. We will very briefly mention a few possible reasons for this poleward propagation in following sections.

Model data allows for a clean and controlled environment that allows the user to control what is being forced. We saw in figure 1 that there is clearly a poleward shift in the reanalysis

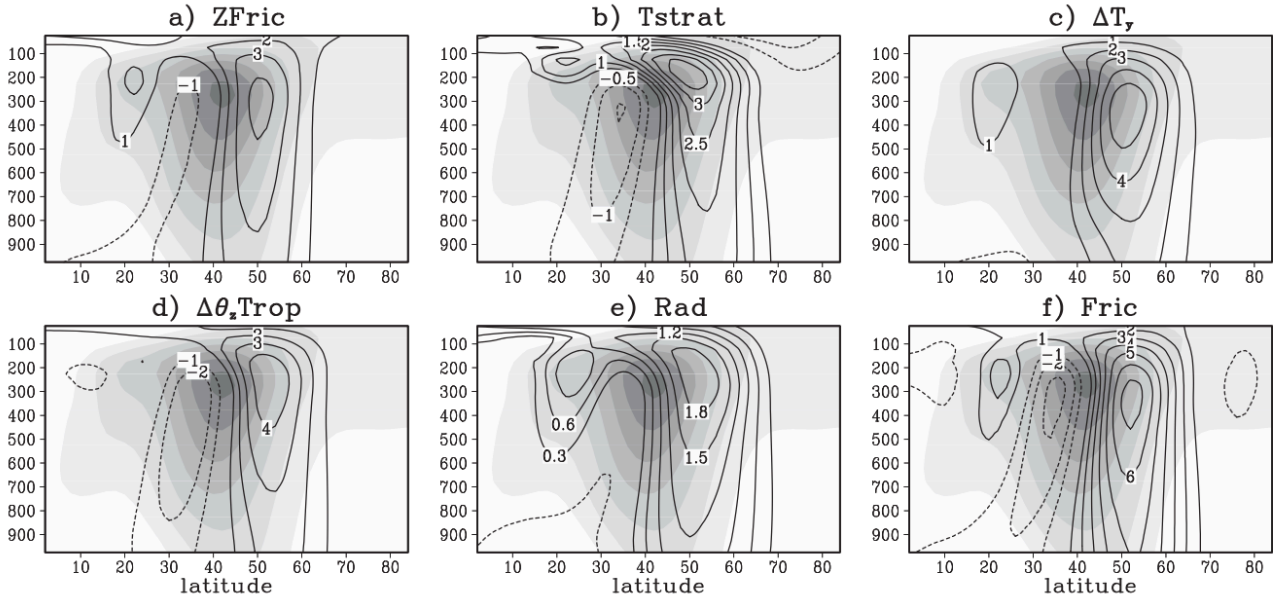

Figure 2. *Fig. 1 from Lorenz (2015) showing 6 perturbed GCM experiments where background shading denotes control run and the change in zonal-mean zonal wind are contoured (ms^{-1}). The x axis is in latitude degrees and the y axis is in pressure (hPa). A) decreases in friction of zonal-mean u B) decrease stratospheric temperature C) increase pole-equator temperature gradient D) increase tropical static stability E) decrease thermal relaxation time scale F) decrease friction.*

data (Feldstein S. B., 1998). Model data also shows a similar poleward trend when forcing a strengthened jet. Lorenz (2015) used a primitive equation model with simplified physics to investigate the relationship between the midlatitude jet and the eddies. In Fig. 2, we see what

happens to the zonal-mean wind when a perturbation is added. The perturbations in Figs. 2a and 2f reduce the friction while the perturbations in Figs. 2b-2e enhance the pole to equator temperature gradient (Lorenz D. , 2015). All of the perturbations in Figs. 2a-2f directly increase the strength of the jet yet they all also lead to a significant poleward propagation of the zonal-mean zonal wind. We will not go into detail on the specifics of this experiment, but it clearly shows that stronger jets shifts poleward. Reanalysis data is another way that we can analyze the potential propagation of the jet stream. Using lagged correlation analysis and reanalysis data, one can directly investigate the poleward propagation of the zonal mean zonal wind and we will be utilizing this strategy here. Previous work shows how this can be done. Lorenz and Hartmann (2001) show that there is clearly poleward propagation of the zonal mean zonal wind by regressing the zonal mean zonal wind onto the principal components of the zonal mean zonal wind. This is shown in Figs. 3a and 3b where the zonal mean zonal wind is regressed on to the second principal component (PC2) of the zonal mean zonal wind at time lag = 0 (Fig. 3a) and time lag = 20 days (Fig. 3b) (Lorenz & Hartmann, 2001). We see that in Fig. 3a, there are high values near the center of the jet at 50°S at lag = 0 which simply shows the atmospheric

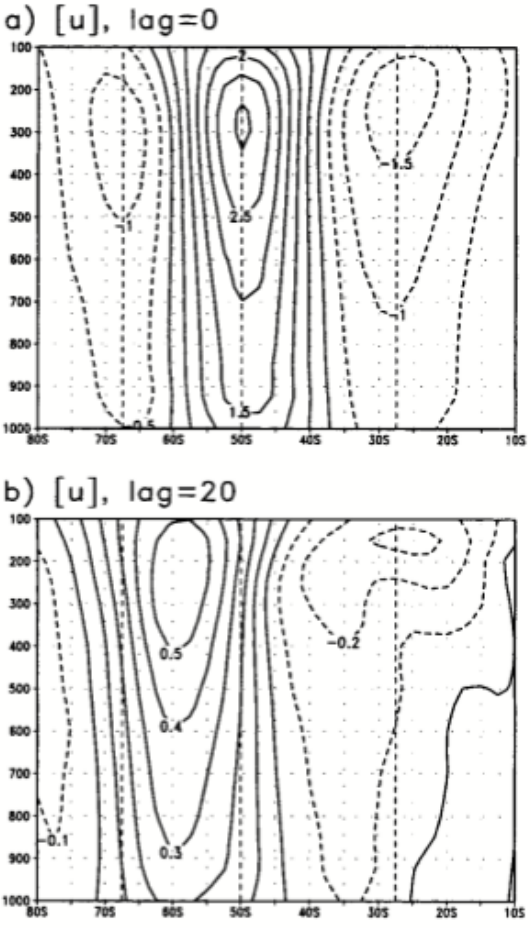

Figure 3. *Fig 15 from Lorenz and Hartmann (2001) showing anomalous zonal-mean zonal wind regressed on PC2 of zonally vertically averaged u when a) simultaneous and b) PC2 leads by 20 days. The dashed vertical lines are the EOF2 wind anomaly latitudes.*

cross section of the zonal mean zonal wind regressed onto PC2. At lag = 20, we see the positive values shift poleward signifying that the anomalies have shifted poleward and further demonstrates a poleward shifting jet. While we will use reanalysis data for the majority of this study, we will briefly use some model data to get an idea of what is going on in a "clean" environment with the ability to control the forcing exactly.

Poleward propagation is also studied in fields besides the zonal-mean zonal wind. For example, Yin (2005) looked at poleward shifts in the storm tracks, which in this case are defined as regions of enhanced transient variability. Not only is there a fairly consistent poleward shift in the storm tracks, a good proxy for the location of the jet, there is also a slight intensification in the jet as well (Yin, 2005). These findings included both the Northern and Southern Hemisphere and while results were more pronounced in the Southern Hemisphere, the Northern Hemisphere did show similar results. Accompanying a poleward shift in the jet is a shift towards the high index state of the NAM and the SAM. In the Southern Hemisphere, there is a poleward shift of baroclinicity that is somewhat offset in the Northern Hemisphere by variation in the meridional surface temperature gradient (Yin, 2005). Studies have used multiple datasets to test the poleward shift of the jet. Riviere used the International Panel on Climate Change (IPCC) coupled models, a three level quasigeostrophic model, and General Circulation Models (GCMs) to see if the jet is indeed shifting poleward (Riviere, 2011). He hypothesized that increases in anticyclonic wave breaking are responsible for the poleward shift. Lorenz (2014) reviews a multitude of possible mechanisms for the poleward jet shift and then tests the mechanisms using a simplified model that calculates eddy momentum fluxes. He concludes that the mechanism involves linear Rossby wave reflection on the poleward flank of the jet. The exact mechanisms and the measure of how much these mechanisms affect the poleward shift of the storm track are

still being examined, but the robust nature of the poleward shift is consistent. The exact mechanisms of the poleward shift are a bit outside the scope of this paper but could benefit from further research.

Unfortunately, there is evidence that the poleward jet shift will continue into the 21st century. CMIP3 20th century simulations of the eddy-driven jet in the Southern Hemisphere show good correlation with the response of the jet to enhanced greenhouse gas forcing scenarios expected in the 21st century (Kidston & Gerber, 2010). The correlation is also significant between the biases of the latitude of the jet and the internal variability of the model when being measured by the annular mode time scale. Studies like Kidston and Gerber are working to model the jet stream using 20th century climatology to help improve the projections of the future of the jet stream in a changing climate. As more models are created and run, the results showing a shifting jet become hard to ignore, especially when these models are run with projected climate conditions. The Coupled Model Intercomparison Project phase 5 (CMIP5) utilizes a multimodal approach which producses consistent results when changing certain parameters, such as increased greenhouse gas emissions. CMIP5 shows that the majority of jets shift poleward with climate change by the end of the 21st century (Barnes & Polvani , 2013). The poleward shift of the jet in the Southern Hemisphere is nearly double that of the Northern Hemisphere shifting by about 2 degrees of latitude when using the representative concentration pathway of 8.5 (RCP8.5) (Barnes & Polvani , 2013). The speed of the jet also increases in the Southern Hemisphere. While RCP8.5 is the IPCC "worst case" scenario for greenhouse gas emissions, it shows that a changing climate will have an effect on the jet stream, likely shifting it poleward. The impacts that a shifting jet can have on variables such as precipitation or temperature are important to

understand for people to physically understand how a shift in the jet will affect them personally. These are tangible effects and the ones that often can lead to changes in perception.

1.3 Impacts of shifting jet on climate

These complex climate models have allowed studies to see the potential future changes of the location and strength of the jet as well as the impacts a shifting jet may have climatologically. Both temperature and precipitation are the primary ways in which people can relate to changes in the climate. Accompanying a poleward shift in the jet stream, there is also a poleward shift in both precipitation and wind stress (Yin, 2005). The strengthening of the poleward shift of baroclinicity in the Southern Hemisphere is somewhat offset by the changes in the surface meridional temperature gradient in the Northern Hemisphere (Yin, 2005). Understanding the behavior of the jet in both hemispheres is critical because there are some important differences in each hemisphere that could affect the zonal-mean zonal wind as a whole. To see some differences in the Northern Hemisphere, some studies divide their results into seasons (Simpson, Shaw, & Seager, 2014). The Northern Hemisphere only shows robust poleward shift in the fall seasons in both Atlantic and Pacific Jets. In fact, in the winter seasons, the jet in the east Pacific shifts equatorward and the jet in the Atlantic strengthens over Europe (Simpson, Shaw, & Seager, 2014). We see here that in a changing climate, the jets will shift in both location and strength, and may do so slightly differently in different seasons and different regions. For now, this research will focus on the jet in the Southern Hemisphere, but with some additional time could be adapted to include the Northern Hemisphere broken up into seasons.

Breaking the jet stream down into the two leading modes of variability provides some significant insight, but also provides challenges and uncertainty when it comes to identifying the

cause or relationship between eddies and the jet stream. While it is understood that the eddies drive changes in the zonal-mean wind, studies want to understand if the zonal-mean wind changes have an effect on the eddy momentum fluxes or if there is a zonal-wind eddy feedback (Lorenz & Hartmann, 2001). One theory as to how a feedback would work here is that there is some baroclinic wave activity in the jet. The wave activity will propagate away from the jet which means that there will be momentum flux into the jet to account for the wave activity lost (Lorenz & Hartmann, 2001). However, this is found to not be the reason of the feedback and it is instead due to the index of refraction of barotropic Rossby Waves (Lorenz D. , 2014). We will not investigate the mechanisms of the feedback further in this paper as the focus will be on quantifying the feedbacks parameters. Through research of the momentum budget, there is a clear positive feedback between the zonal-wind anomalies and eddy-momentum fluxes in both the Northern and Southern Hemisphere (Lorenz & Hartmann, 2001) (Lorenz & Hartmann, 2003). A common strategy for looking at the modes of variability is through Empirical Orthogonal Function (EOF) analysis. Kisdon (1988) used EOF analysis to look at the zonal indices of the Southern Hemisphere zonal wind (Kisdon, 1988). EOF analysis is adept at picking out the leading modes of variability from data in which that would be incredibly challenging to do. It has been used to study the zonal-mean wind and eddy momentum flux feedback (Lorenz & Hartmann, 2001) (Lorenz & Hartmann, 2003) (Eichelberger & Hartmann, 2007). We will attempt to use EOF analysis in further investigating the eddy-flow feedback in this paper.

1.4 Evidence for Eddy-Flow Feedback

Understanding how the eddy-flow feedback affects the jet stream is critical in this study. Remember, the zonal index refers to the dominant mode of variability in the jet. There is

evidence that the zonal index dominates in the summer season for both hemispheres and also the winter season in the Southern Hemisphere (Feldstein & Lee, 1998). When dealing with eddies, it is important to look at different frequencies because feedbacks can occur at different timescales. When dividing the eddies into different frequency bands, the evidence shows a consistent eddy feedback by the high frequency (period of less than 10 days) transient eddies (Feldstein & Lee, 1998). The presence of these eddies prolongs the zonal index anomalies for both low and cross (product of high and low) frequency eddy forcing (Feldstein & Lee, 1998). A simple atmospheric model corroborates the importance of the frequency in the eddy forcing. Eddy feedback is positive for low-frequency variability in the zonal flow, but is negative when the frequency period is less than a month (Robinson, 1994). There is a feedback here between the eddies and dominant mode of variability in the jet stream and we hope to investigate this further using also the second mode of variability.

1.5 Objectives

The focus of investigation in this paper is the eddy-flow feedback, but it is different from previous studies in one key way. We will look at the eddy-flow feedback using a two-mode approach. Most previous studies look at just the leading mode of variability, but we will be using both the leading mode of variability and the second leading mode of variability. Feldstein and Lee (1998) found that to identify the poleward propagation of the jet, using two modes was necessary. Using two modes provided evidence to prove that an eddy feedback was present with the high-frequency transient eddies (Feldstein & Lee, 1998). Also, a response to external forcing suggesting stronger jets shifting poleward requires a coupling between changes in phase with the jet and out of phase with the jet, or EOF2 and EOF1 respectively. We will use EOF analysis as

the primary statistical tool in an attempt to quantify the feedback between the eddies and the zonal mean flow for both of the leading modes of variability (EOF1 and EOF2). Careful EOF analysis is key when working with the two modes because there are many interactions to consider. Instead of just looking at the dominant mode of variability and quantifying the feedback between the zonal wind and the eddy flux convergence, we will be looking at quantifying the feedbacks for each of the two modes for each of the two variables giving us four feedback parameters. We will also investigate the seasonality of these feedbacks

2. Methods

The focus of this study is to quantify the feedback parameters of zonal mean wind and eddy-momentum flux using the two dominant modes of variability. To accomplish this, we will primarily use EOF analysis and lagged correlation analysis. In section 2.1, we will introduce in greater detail the use of EOF analysis to explain why this is the best tool for this research question and what concerns using EOF analysis may bring to light. The next two sections, 2.2 and 2.3, will introduce the datasets we used in this investigation. We use both a synthetically generated dataset along with reanalysis data. The final section, 2.4, will carefully explain the steps taken to transform the raw yearly data into more manageable pieces through reducing the dimensionality and dividing into seasons. We will also discuss the necessary weighting, removal of mean annual cycles, and addition of buffers necessary to make sure that the EOF analysis could be used effectively on this data.

2.1 Empirical Orthogonal Functions (EOFs)

The study of the atmosphere is unique in that it not only requires high dimensional data, but it also requires that the data be processed quickly (Monahan, Fyfe, Ambaum, Stephenson, & North, 2009). EOF analysis has been used in the study of the atmosphere since the late 1940's (Obukhov, 1947). EOFs allow for the decomposition of high dimensional data from a field that contains time and space into spatial patterns and time indices accomplishing the goal of reducing dimensionality (Hannachi, Jolliffe, & Stephenson, 2007). A known challenge when studying the atmosphere is the presence of both propagating and stationary features. With these challenges present, EOFs are not a perfect tool to use when studying the atmosphere and can be tough to interpret. EOFs have some geometric properties and orthogonality in space and time that makes the interpretation difficult. One way to handle high dimensional data is through careful use of statistical techniques that can reduce the dimensionality. Empirical orthogonal function (EOF) analysis is one way to attack a complex atmospheric dataset which allows for this key reduction of dimensionality. EOF analysis is popular for a number of reasons according to Weare and Nasstrom (1982). One reason is that EOF analysis describes variations of complex geophysical fields with few functions and time coefficients. Another reason they give is that EOF analysis works well with any variable observed on any grid (Weare & Nasstrom, 1982).

One must be cautious though when using EOF analysis, or any statistical technique for that matter, as statistics tend to leave a biased imprint on the output (Monahan, Fyfe, Ambaum, Stephenson, & North, 2009). For EOF analysis, this imprint can lead to some challenges when trying to understand the physical and dynamical components of the dataset. EOF analysis does contain some bias that must be considered, but it can also be extremely valuable in understanding the spatial structures and which ones carry the most variance (Monahan et al, 2009).

EOF analysis provides EOFs and principal components (PCs) that can be converted into power spectra and ultimately lagged correlation. Lagged correlation analysis more clearly shows how the different modes are connected or correlated. Lagged correlations can be used to highlight dynamical affects and can do well with stationarity, but may struggle when dealing with propagating features (Byrne, Shepherd, Woolings, & Plumb, 2016). Positive lagged correlations between two variables shows that they are varying together identifying these correlations are important. Negative lagged correlations are important too as they show relationships that are out of phase compared to the positive lagged correlations which are in phase relationships. Using lagged correlations to distinguish between the presence of eddy feedbacks and nonstationary interannual variability is a known challenge that could use further research (Byrne, Shepherd, Woolings, & Plumb, 2016). There is also significant seasonal dependence on lagged correlations. We hope to investigate the correlations between the two modes in the eddy-zonal flow feedback and see how they change when there is no feedback present for both full and seasonal data.

The benefits of using a conventional EOF analysis are easy computation and efficient data reduction along with containing some useful geometric properties. The deficiencies of the conventional EOF analysis are the predictable relations between EOFs and the interpretability of physical features. The other types of EOF analysis are REOFs, simplified EOFs, extended EOFs, and complex EOFs (Hannachi, Jolliffe, & Stephenson, 2007). But each type of EOF analysis does have some deficiencies. For example, rotated EOFs (REOFs) may be used as an alternative to EOFs and can identify more local features but cannot handle propagating features. All of these different types of EOFs contain some benefits to go along with some deficiencies.

The research here uses different datasets to glean important information about the research question. We will first briefly explain each set of data we will use in the paper and then get into how we plan to use each dataset to get results.

2.2 Synthetic data

Before working with the ERA-Interim data, we realized that the best way to back out an unknown feedback parameter would be to generate a synthetic dataset with an imposed feedback. With a known feedback, we can work backwards using our methods to see if we can accurately back out the feedback parameter(s) that we imposed. A synthetic dataset of the same size as the observed data will be useful in corroborating our statistical techniques with consistency. By creating the same size synthetic dataset, it will be easy to simply change the input data from the synthetic data to the reanalysis data once we know that our methodology is sound. It is important to note that we are not creating specific wind and eddy momentum flux values in a traditional sense. Instead, we are creating zonal-mean wind and eddy momentum flux principal components that mimic the principal components we use in the EOF analysis of the ERA-Interim data. The most basic synthetic dataset we create uses Equation 1 below:

$$\frac{du}{dt} = r - \frac{u}{\tau} \qquad \textbf{Equation 1}$$

where u is the zonal wind, τ is the damping timescale primarily due to surface friction, r is the random eddy forcing, and t is the time.

Equation 1 represents the vertical and zonal-mean momentum budget. The Coriolis term (f*v) disappears because it has equal and opposite signs in the upper and lower troposphere. This leaves us with Eq. 1 which simply shows that u is forced by the eddy momentum flux convergence (m) and friction (u/τ). The r in these equations has the same length (55520, all

time steps) as the principal components of EOF 1 and EOF 2 of the ERA-Interim data. We set τ to be 8 days, which is a reasonable value for damping rate of friction on the vertically averaged flow. We can use the data generated here to plot the auto correlations and the correlations between the eddy momentum flux and the zonal mean wind Once we can create our most basic synthetic dataset, we can build on it by adding feedbacks. First, we will just add one feedback parameter.

When we induce a feedback (see Table 1 for a11), the only difference to the original equation is the addition of a feedback term, which in this case is *au* where *a* is the feedback constant and *u* is the same u in Eq. 2. The single feedback case is the only one considered so far in literature (e.g. Lorenz & Hartmann, 2001). Eddy forcing has two components: a random component and a component that is dependent on u. We know that $a > 0$ means that eddies are not purely random but a component of eddy forcing reinforces the u anomalies and vice versa for $a < 0$.

$$\frac{du}{dt} = m - \frac{u}{\tau} \qquad \textbf{Equation 2}$$

where $m = r + au$.

The last thing we do to this synthetic feedback is create a two-mode feedback to allow the possibility the EOF1 is coupled to EOF2, which is consistent with the poleward propagation of u anomalies seen in observations (Feldstein S. B., 1998). When we add a second mode to both the zonal-mean zonal wind and the eddy forcing term, we get a matrix equation as seen in Equation 3, which is still quite similar to Eq. 2.

	U1	U2
M1	$a_{11} = \frac{1}{3}\tau$	$a_{12} = \frac{2}{3}\tau$
M2	$a_{21} = -\frac{2}{3}\tau$	$a_{22} = 0$

Table 1. *Imposed feedbacks for Synthetic Data.*

$$\begin{pmatrix} \frac{du_1}{dt} \\ \frac{du_2}{dt} \end{pmatrix} = \begin{pmatrix} m_1 \\ m_2 \end{pmatrix} - \frac{1}{\tau}\begin{pmatrix} u_1 \\ u_2 \end{pmatrix} \quad \textbf{Equation 3}$$

where the subscripts denote Mode 1 and Mode 2 and $m1\ and\ m2$ are explained:

$$\begin{pmatrix} m_1 \\ m_2 \end{pmatrix} = \begin{pmatrix} a_{11} & a_{12} \\ a_{21} & a_{22} \end{pmatrix}\begin{pmatrix} u_1 \\ u_2 \end{pmatrix} + r \quad \textbf{Equation 4}$$

When we create a two-mode feedback, due to the matrix aspect of Eq. 3, we are actually creating 4 feedback parameters (see Eq. 4). To generate these synthetic datasets, we have to impose our own feedback parameters into the equations for the zonal wind and eddy momentum flux data seen above. Table 1 shows the feedback parameters we used and how they are connected each of the two modes of u and m. We choose these feedback parameters because they were somewhat close to the actual feedback parameters we found with our reanalysis data. By choosing feedback parameters to impose that were close to the actual feedback parameters we found, we can more confidently compare between the two cases. We could have run the synthetic data case with exactly the same feedback parameters we found but chose not to for one main reason. It does not matter exactly what the feedback parameters are in the synthetic data case because we use this dataset as a proof of concept. If we can back out the imposed feedbacks accurately, we know we will be able to do the same with the reanalysis data, but the actual feedback parameters are not as important as the process. We will use the same τ for each mode in this case, but we should note here that the τ will be slightly different in each mode in our reanalysis data. We will show the difference in τ for the two modes in later analysis. Because we know exactly what our feedback parameters are, we can use some statistics to back out the feedback parameters and test our methodology. If we cannot replicate the parameters exactly, we will have to change our statistical techniques to make sure we can replicate them. If we can

replicate them, we know that our methodology is sound, and we should be able to back out each of the feedback parameters from the ERA-Interim data.

2.3 Observed data

For this study, the primary dataset we used for analysis was the ERA-Interim (European ReAnalysis) generated by the European Centre for Medium-Range Forecasts (ECMWF). The ERA-Interim dataset provides a new and improved version of the ERA-40 dataset, a sophisticated atmospheric reanalysis (Dee, et al., 2011). This reanalysis provides a plethora of atmospheric variables useful to understanding the atmosphere. For this study, we will focus on using the wind, both zonal (u) and meridional (v), for all points on the specified grid. While meridional wind will not be investigated directly, it will be used through an eddy momentum flux term which is a product of zonal and meridional wind. The variables are in the form of 4 x daily data (or 6-hourly) with 18 pressure levels (1000,925, 850, 775, 700, 600, 500, 400, 300, 250, 200, 250, 100, 70, 50, 30, 20, and 10 mb) on a grid with 240 longitude points and 121 latitude points. The time dimension covers a span of 39 years from 1979 to 2017. This is a much more recent dataset than the older ERA-40 which covers more time but is not as recent as it goes from 1957 to 2002. The ERA project does have one dataset that does cover over 100 years in the ERA-20C dataset, but the early years include sparse data as observations were less reliable due to limited coverage by observing stations. ERA-Interim is the most recent dataset and the most robust giving us a good dataset to run our study with. Before moving forward with using this data, we must make a note of the way we took the raw yearly data and formulated it into a way that we could use it effectively and efficiently.

2.4 Setting up the Data

We need to create zonal and vertical averages u before we do the analysis of the ERA-Interim data. We use the zonal and vertical average of u becuse the momentum budget in this case is very simple. Therefore, it is easy for us to isolate the effect of the eddies on u. For example, if things depend on longitude, we still have meridional eddy momentum fluxes, but advection by the mean flow itself could change the location of the resulting u anomalies forced by the eddy momentum fluxes. In addition, there are other terms that are involved if we do not take the zonal and vertical averages which could make it difficult to identify the effect of eddies on u. A fringe benefit of taking the zonal and vertical averages of u is that we do reduce the size of the data significantly making computations significantly easier and faster.

Since we do take the zonal averages, we lose the ability to investigate specific regions because we only focus on the latitude, but there are some studies that have looked at the regional evidence and effects of a shifting jet. These regional investigations of the shifting jet are important as they can key in on the specific impacts a shifting jet may have on each region, which may be different from region to region. For example, the positive phase of the SAM decreased geopotential height in the midlatitudes and strengthened the poleward shift of the storm tracks (Thompson & Wallace, 2000). The effects of this positive phase are linked to a significant cooling over Antarctica and Australia, but a warming over the Antarctic Peninsula, Argentina, Tasmania, and southern New Zealand (Gillett, Kell, & Jones, 2006). The regional impacts of precipitation also show dry conditions over South America, New Zealand, and Tasmania, but wet conditions over Australia and South Africa (Gillett, Kell, & Jones, 2006). These are just a few examples of the impacts that the shifting jet may have on specific regions, especially in a changing climate. It is important to understand the regional behaviors of the jet

and the impacts, but for our study, we will be focusing on the zonal mean jet and how it varies in a changing climate.

2.4.1 Removing Mean Annual Cycle

A key step we have to take when working with this data is removing the mean annual cycle. We remove the mean annual cycle because there is so much variability due to the seasons that we do not want that variability to interfere with the internal variability specifically linked to the jet and eddy interaction. Without removing the variability, the dominant mode of variability would undoubtedly be the seasonal variability. To remove the mean annual cycle, we find the average over 39 years for each calendar date in the record. Because each calendar date has 4 time steps due to the 6-hourly data, we have four separate averages for each date (00, 06, 12, and 18 UTC). For example, this means that all data points for January 1 at 12 UTC over all 39 years are placed in an annual dataset. This will give us 39 data points at each time for a full year. We can take the mean at each time step in this full year of data to get a mean annual cycle dataset made up of the means for each time step. Once we have our mean annual cycle created, we smooth it. The reason for smoothing the mean annual cycle is because while 39 years is a robust time period, there can still be some noise in the mean annual cycle. We use a 30-day moving mean to smooth the mean annual cycle. We properly account for the idea that the mean annual cycle is periodic in time when we smooth the mean annual cycle. With the mean annual cycle calculated and smoothed, we can then simply subtract it from the original dataset to get the anomalies. Anomalies of the data will help give us more useful information on the variability of the zonal mean wind and the eddy momentum flux feedback as we do not have to worry about seasonal variability interfering with the variability we are trying to investigate.

2.4.2 Momentum Flux Convergence

Using the ERA-Interim zonal wind and meridional wind, we calculate the eddy momentum flux. We do so by removing the zonal mean u and v to find the eddy u and v which we will denote by u' and v'. Then we multiply u' and v' together and zonally average to get the eddy momentum flux which we denote as $\overline{u'v'}$.

Once we have $\overline{u'v'}$, we can use an equation to convert from $\overline{u'v'}$ into the eddy momentum flux convergence (denoted by m) which we will use in our analysis. Note the $\overline{u'v'}$ here is also vertically averaged when doing this calculation (see next section). The equation we use to convert this into a flux convergence is a form of centered differencing that uses the cosine of latitude. We use the exact derivative form of this equation and we use standard order centered differences to approximate, except at the poles where first order differences are used. The equation we use here is:

$$m = -\frac{1}{(Re*cos(\theta)^2)} * \frac{d(u'v'*cos(\theta)^2}{d(\theta)} \qquad \textbf{Equation 5}$$

where θ is latitude and Re is the radius of the earth, and m is the eddy momentum flux convergence.

This equation takes the difference of $\overline{u'v'}$ at one latitude on either side of the latitude we are looking for and divides by the area between the two latitudes. To make the m values more intuitive, we convert m units to m/s/day by dividing by the number of seconds in a day. By converting into per days, we get a better sense for what the eddy momentum flux convergence is doing on a daily timescale. Note here that we will be using m to refer to the eddy momentum flux convergence for the rest of this paper.

2.4.3 Vertical averaging, Weighting, Daily Means

Once we remove the mean annual cycle, we take the vertical average from 1000mb to 100mb and weight by mass. The averaging is confined below 100mb because, the stratospheric dynamics at those levels have the potential to interfere with our results and could introduce variability that is completely different than the variability we are looking to identify. When performing EOF analysis, the data is additionally properly weighted by latitude to take into account the decrease in area towards the poles (e.g Lorenz & Hartmann, 2001). Moving forward, we will perform EOF analysis on the daily mean u values. We will still use the original 6-hourly data as they will be projected onto these daily EOF patterns to produce 6-hourly PCs that we will use for our lagged correlation analysis.

2.4.4 EOFs to get Principal Components

Now that we have all of our data in the correct forms, we can start our EOF analysis. The first thing we need to do is perform a singular value decomposition which will produce the EOFs, Principal Components (PCs) and a diagonal matrix of singular values. In our case, the input is the cosine weighted, vertically averaged zonal wind (denoted as $\overline{u'}$) and we chose an arbitrary amount of EOFs to be 20. We will only be looking at the first 2 EOFs for our analysis. The first two modes explain the most variance, but the amount of variance explained drops off with each mode. Note that we do not do EOF analysis directly on $\overline{u'v'}$. We project $\overline{u'}$ and $\overline{u'v'}$ onto the EOF patterns we calculate from the daily $\overline{u'}$. The equations we use to project the data onto our EOFs are:

$$PC\ u1 = \sum \frac{\left(EOF1(nt) * \overline{u'}(nt)\right)}{ny} \quad \textbf{Equation 6}$$

$$PC\ u2 = \sum \frac{\left(EOF2(nt) * \overline{u'}(nt)\right)}{ny} \quad \textbf{Equation 7}$$

$$PC\ m1 = \sum \frac{\left(EOF1(nt) * \overline{u'v'}(nt)\right)}{ny} \quad \textbf{Equation 8}$$

$$PC\ m2 = \sum \frac{\left(EOF2(nt) * \overline{u'v'}(nt)\right)}{ny} \quad \textbf{Equation 9}$$

where $ny = 48$ for the number of latitude points between 81°S and 10.5°S.

It is important to emphasize a point made earlier regarding the use of daily and 6-hourly data. The EOF1 and EOF2 in Eqs. 6-9 are generated using the daily $\overline{u'}$ and the $\overline{u}'$ and $\overline{u'v'}$ terms in those equations are the 6-hourly data. We calculated the EOFs using daily $\overline{u'}$ and this is the only time we really use the daily $\overline{u'}$. We project the 6-hourly $\overline{u'}$ onto the EOFs to make sure that our PCs are in the form of 6-hourly data. One reason to use 6-hourly data when creating the PCs is that daily mean data has trouble capturing the eddy feedback due to medium scale waves. Medium scale waves play an important role on the variability of the SAM. SAM is supported by a positive feedback between the zonal mean wind and the eddies and about two thirds of that feedback comes from synoptic waves and the other one third comes from medium scale waves (Kuroda & Mukougawa, 2011). Medium scales waves may have smaller climatological amplitudes than synoptic waves, but their influence is significant, especially at short timescales, and therefore, we must take that into account and use the 6-hourly data in our PCs. While we use the daily means to create the EOFs, we still need to use the 6-hourly data to project onto those EOFs to get the PCs.

Because the sign of EOFs are arbitrary, we impose the following sign convention on the EOFs so that results are easy to compare across seasons: a) EOF1 is positive poleward of the jet and negative equatorward of the jet and b) EOF2 is positive at the latitude of the jet. Also, the

EOFs shown here are given in units of the corresponding field by projecting the original anomalies on the normalized PC time series.

2.4.5 Adding Buffers for Seasonal Analysis

Once we have the PCs, we will begin the process of working towards lagged correlation analysis, but we have to make a note of one small but important step in which we add buffers to the end of our seasonal analysis due to assumptions implicit in Fourier decomposition. We will calculate power spectrum from the PCs and then convert power spectrum to lag covariances and eventually, lagged correlations. Using lagged correlations will allow us to interpret our results in a more meaningful manner and also provide the opportunity to calculate the feedback parameters. However, certain calculations will be easier to do in Fourier, or frequency, space. To ensure complete consistency between spectral (power spectrum) and temporal (lagged covariances, correlations) analysis, power and cross spectra are computed first and then we directly compute lagged covariance from the spectra using Fourier transform. Because a Fourier decomposition implicitly assumes time series are periodic, cross covariances at nonzero lags computed using a Fourier transform are contaminated because the start and end of the time are assumed to be adjacent. To account for this adjacent assumption, we add a buffer of zero values with a length of at least the number of lags to each season prior to spectral analysis to prevent the contamination.

3. Results

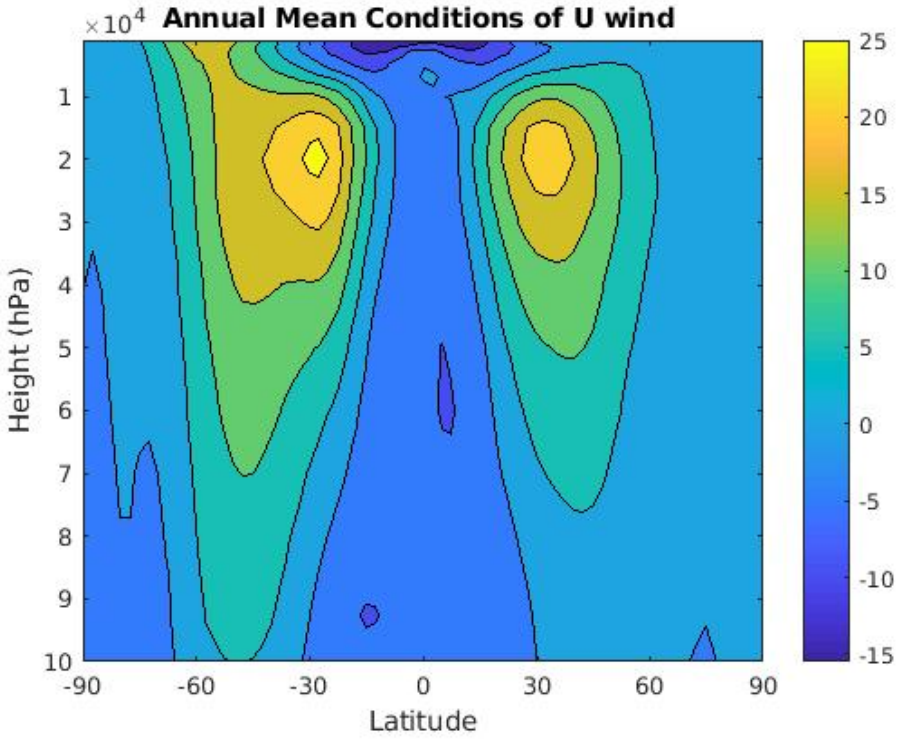

Figure 4. *Mean annual conditions of zonal (u) wind from ERA-Interim data measured in* ms^{-1}.

Before we begin to run our statistical analysis to investigate the variability in the zonal-mean, it would be beneficial to look at the what the annual mean state of the zonal wind looks like in an atmospheric cross section using the ERA-Interim data (Fig. 4). This is important to point out the key features before running our statistical analysis because this will help provide more of a full picture of what the zonal wind looks like for the annual mean of the ERA-Interim data. We can now view the zonal wind with respect to vertical height and latitude. In Fig. 4, we see two significant peaks in wind speed in two locations, about 30°S and about 35°N. These signify the two main jets that we see in the Southern and Northern Hemisphere, respectively. We should note here that the zonal jets for any given day are the subtropical and the polar jets, but when we take the zonal-mean zonal wind, they are averaged out. Also, note the extension of the jet in the Southern Hemisphere to about 50°S. The jet located at 30°S is called the subtropical jet, where the zonal wind is the strongest, and the jet

located at 50°S is the mid-latitude jet. Later, we will weight with respect to the vertical dimension. From here on out, we will almost exclusively be view the variability of the zonal wind with respect to just latitude. In figure 5, we see the zonal mean u wind for both hemispheres at two different levels (250mb and 850mb). The levels chosen are arbitrary and meant to provide an example of how the jet appears in a zonal-mean sense as we move forward

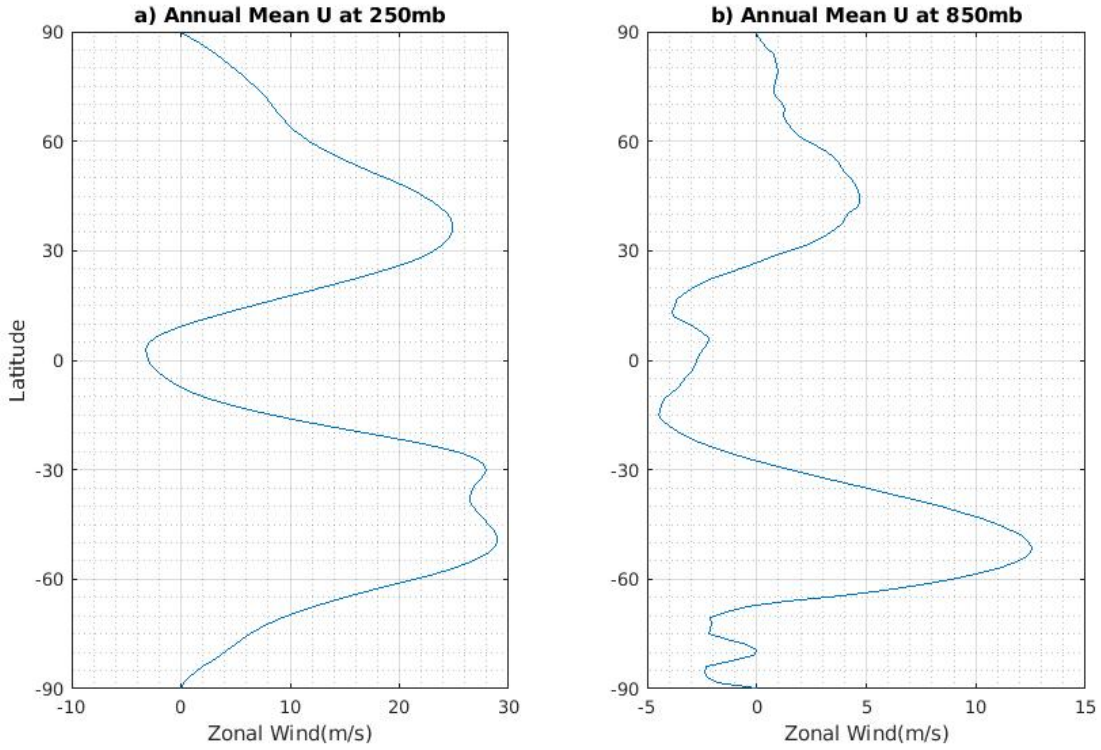

Figure 5. *Annual mean zonal (u) wind at a) 250 mb and b) 850mb.*

in the analysis. As we see in figure 4, figure 5 also clearly shows the location of the major jets in each hemisphere for both levels sampled here. Both Figs. 4 and 5 show a relatively stronger Southern Hemisphere jet than Northern Hemisphere. We can note here that the jet is stronger in the upper level (250mb). The mid-latitude jet is where there tends to be the strongest zonal winds at the surface. The subtropical jet is tightly linked to the heating gradient between the tropics and the subtropics (Lorenz and Hartmann, 2001). Thus, most of the variability in the

subtropical jet is due to the seasonal cycle of heating in the tropics where we see a strong jet in the winter and a weaker jet in the summer. We will focus on the mid-latitude jet because the eddies are the most important for this jet. Eddy activity is created by the instability linked to the temperature gradient of the lower levels of the mid-latitudes (Lorenz and Hartmann, 2001). The ocean plays a large role in maintaining this gradient and in the Southern Hemisphere, where the oceans dominate, the seasonal cycle is much smaller than in the Northern Hemisphere. This means most of the variability in the zonal-mean zonal winds is largely due to internal dynamical processes and not due to the external seasonal cycle (Lorenz and Hartmann, 2001).

3.1 Synthetic Data

Once we have a general understanding of the basic jet structure and how to set up the EOF analysis, we can use a synthetic dataset to compare against the ERA-Interim data which will be seen later. The benefit of using a synthetic dataset is that we can relatively easily impose feedbacks to the dataset which will give us the opportunity to see if we can correctly back out the feedback parameters. We do not use the synthetic data to investigate the EOF structure because we start with generating the principal components used in lagged correlation analysis.

3.1.1 Lagged Correlation Analysis

Because the synthetic data created is already in the form of PCs, we can begin with the lagged correlation analysis. With the reanalysis data, we will go through the EOF analysis from the original data to produce the PCs which we do not do here. Note here that the synthetic data in this section is generated from Eq. 1 where m is random noise and u is generated from Eq. 1. Figure 6 shows the lagged auto correlation of the *u* and lagged auto correlation of *m* and the lagged cross correlation *u* and *m*. Note that the two auto correlations only show the positive lags, but are mirrored identically in the negative lags. By definition, an auto correlation is correlating one variable with itself and so since the variable is the same, the correlation will be the same at corresponding positive and negative lags. The first thing we notice is that the u auto correlation

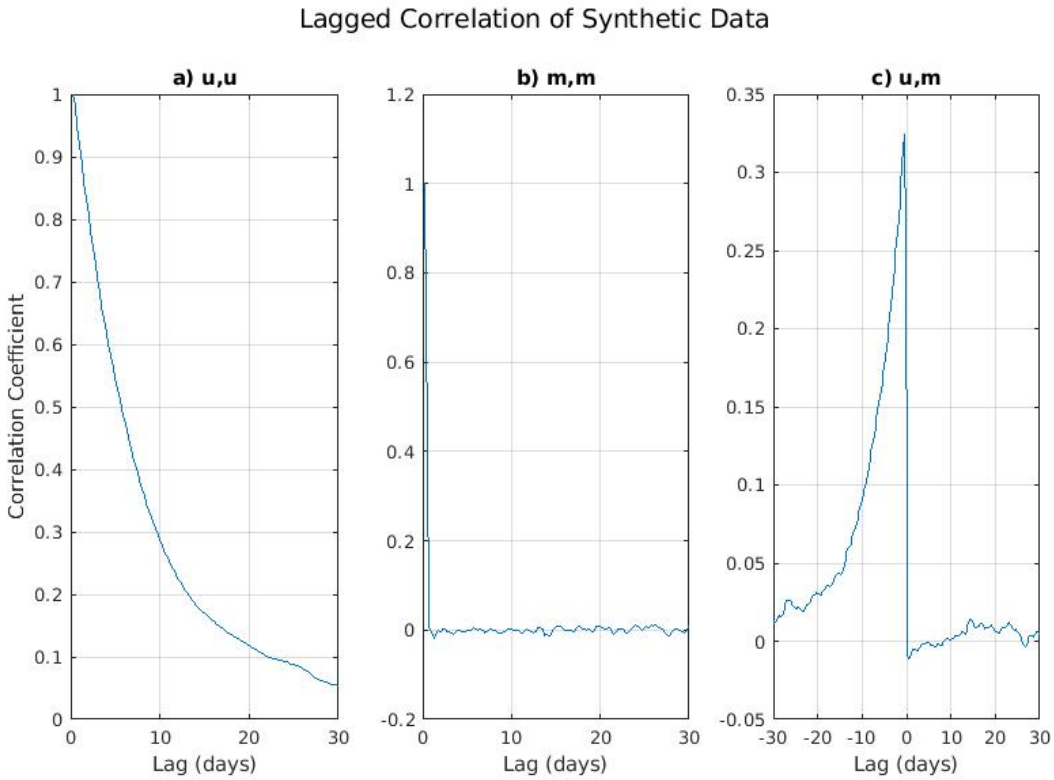

Figure 6. *Lagged correlation analysis of Synthetic data with no feedback. A) Auto correlation of u B) Auto correlation of m C) Cross correlation of u and m when at negative lags m leads u and at positive lags u leads m.*

drops down to zero correlation after about 30 days. Since we generate the u from Eq. 1, you can see that there will be some correlation between different lags of u. On the other hand, the auto correlation of m shows an initial value of 1 at lag = 0, but immediately drops to zero correlation. This is what we would expect because the m is completely random so there is no connection from point to point. But when we use Eq. 1 to get u, there is some correlation between different u values up until lag = $\pm$ 30 days. We gain some significant insight when looking at the cross correlation between u and m and this relationship will be an important focus in our reanalysis data. When m leads u, the correlation is high at short negative lags and drops towards zero near lag = -30 days. The strong correlations at short negative lags are a result of the eddy momentum flux forcing the zonal wind (Lorenz & Hartmann, 2001). The reason for the relatively large

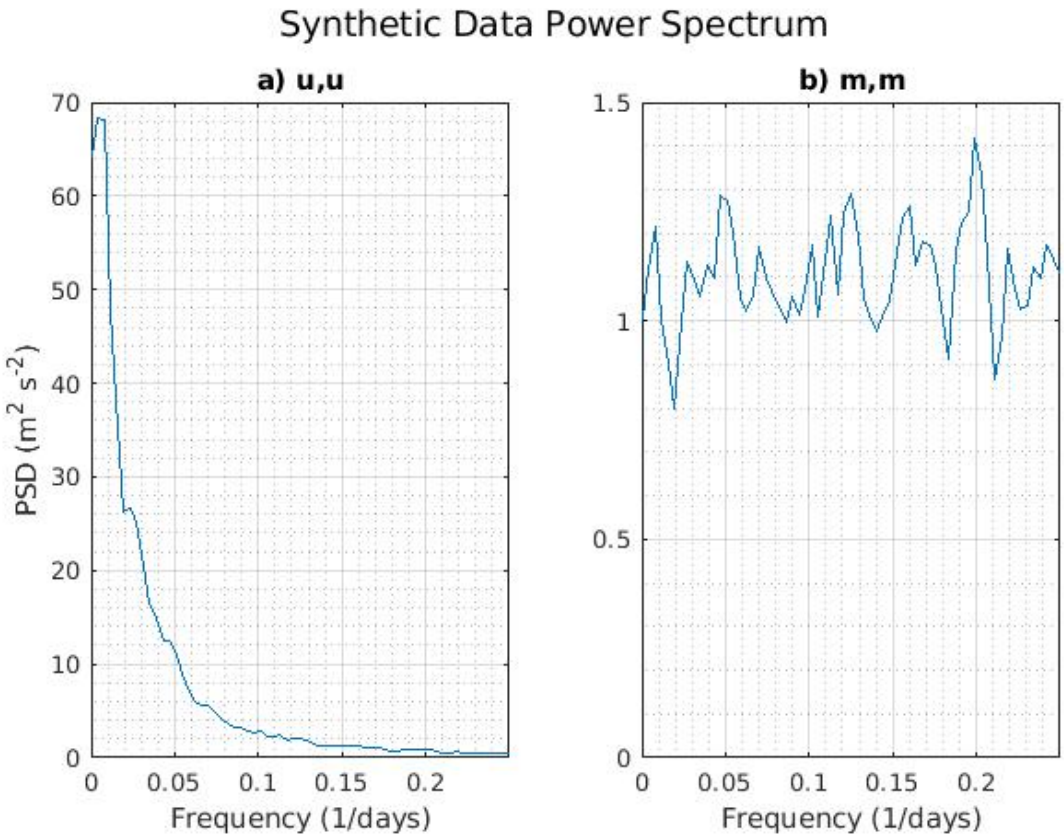

Figure 7. *The power spectrum for the synthetic data with no feedback. A) Power spectrum of u and B) Power spectrum of m.*

magnitude of the correlation at the short lags is due to the differences in the timescales of u and m (Lorenz & Hartmann, 2001). However, when u leads m, the correlation is zero at positive lags, which is expected. We expect this to be the case because m is forcing u. At negative lags, Fig. 6c shows the correlations when m leads u. This has high correlation values near zero because m forces u. At positive lags in Fig. 6c, u leads m and because m forces u in the generation of this dataset, there is no correlation in the other direction. We can also look at the power spectra for each variable as well to see what frequencies of the signal have the highest power. In Fig. 7, the key observation is that the timescale of u is much longer than the timescale for m. Also, the power spectrum for m, is quite random in this case and there is not much we can take from this. There is a slight peak of m around 0.2 per day but it is not robust. Because m is completely random, we can assume this is purely an artifact and due to the random noise. In the cases where we add feedbacks, we will be looking primarily at how the correlations change. We conserve all of the information present in the power spectra through Fourier series when converting to correlation and could learn something from the power spectra, but it will be much easier moving forward to focus on the changes in correlations to gain insight.

When we add a feedback to the synthetic data, the correlations may appear to change only slightly, but this change is important. In Fig. 8, we see a similar pattern in the correlations when we add a feedback to the pattern in the no feedback original case. In the auto correlation of u, the correlation at high lags drops down as it did before, but it does not drop all the way down to zero in the 30 days. The auto correlation for M is perhaps more telling in that instead of going to zero after lag = 0, there is a slight positive correlation. Before we added a feedback, m forced u but the opposite was not the case (u did not force m). When we add the feedback, we use Eq. 2 where m forces u and additionally u feeds back on and alters m (see m term in Eq. 2). There

is a positive correlation of u and m which is higher at the lower lags and slowly trails to zero. We can see this a bit more exaggerated in the cross correlation of u and m. The addition of a feedback has an affect that produces positive correlations at small lags. We will be focusing on identifying these non-zero correlations at large positive lags because non-zero correlations at these longer lags are evidence of a feedback. We must note a key point to understand why this is evidence for a feedback. The correlations at positive lags only imply a feedback if we assume that m inherently by itself has no long-term persistence, which is a given due to the random data we started with. Then we can say that with this assumption, correlations at positive lags mean that m anomalies are persisting after they force u. Because this persistence cannot come from

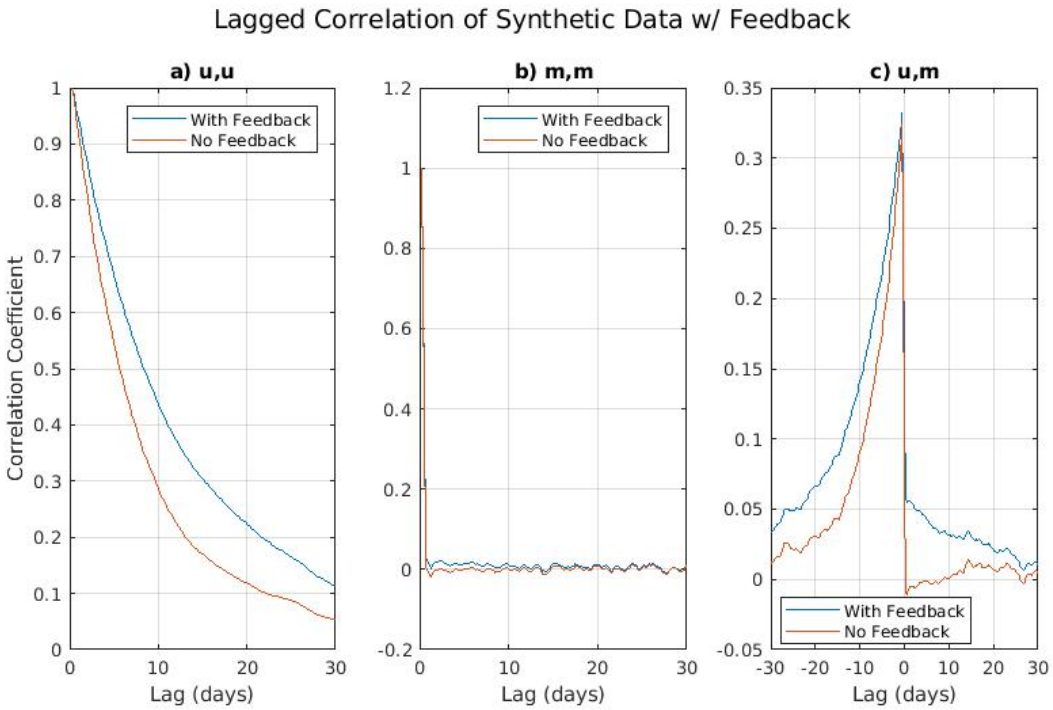

Figure 8. *Lagged correlation analysis of synthetic data with a feedback (blue) and with no feedback (red). A) Auto correlation of u B) Auto correlation of m C) Cross correlation of u and m where at negative lags m leads u and at positive lags u leads m.*

the eddies themselves, it must be coming from somewhere else. Because the u anomalies persist, the most prudent hypothesis is that u is also affecting m and this leads to the persistence of m anomalies in the u and m lagged correlation.

Adding a second feedback introduces more cross correlations to compare how the modes, or feedbacks, impact the others. For example, if we just look at the auto correlations for $u1, u2, m1$ and $m2$, we do not see much difference in the general shape of each auto correlation. In Fig. 9, we see that $u1$ is similar to the one mode auto correlation of u in that the correlation is high at lag = 0 and drops to zero by lag = 30. However, the $u2$ drops below zero around lag = ±16 days. The reason for this going negative is not immediately clear but this is the main

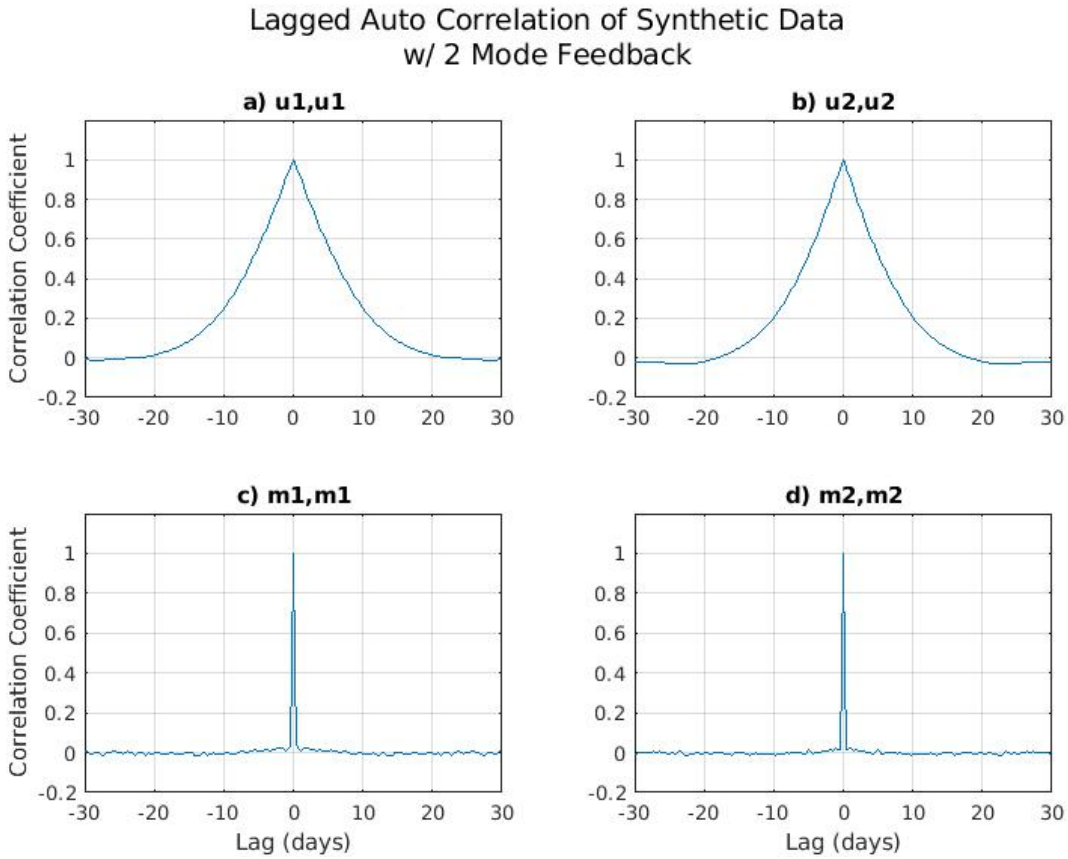

Figure 9. *Lagged Correlation analysis of synthetic data with two mode feedback. A) Auto correlation of u1 B) Auto correlation of u2 C) Auto correlation of m1 D) Auto correlation of m2*

difference in the auto correlations of u when adding a second feedback. The $m1$ and $m2$ auto

correlations are nearly identical. We should also note that at low lags, like we saw in the one mode feedback, the $m1$ and $m2$ correlations are small but positive. The cross correlations when adding a second feedback will tell us more about how the zonal wind and the eddy momentum flux are related across two modes. In Fig. 10, we see the cross correlations for 6 different pairs of the two modes of u and m ($u1u2, u2u1, m1u1, m1u2, m2u1, m2u2$). Note here that $u1u2$ and $u2u1$ are exactly opposite. From here on, we will only show $u1u2$ for simplicity. These are the 6 pairs and corresponding correlations that we will be most interested in. First, we will discuss the cross correlations between $m1u1$ and $m2u2$. The cross correlations of these two plots are nearly identical. The negative lags in this case show $m1$ leading $u1$ and the positive

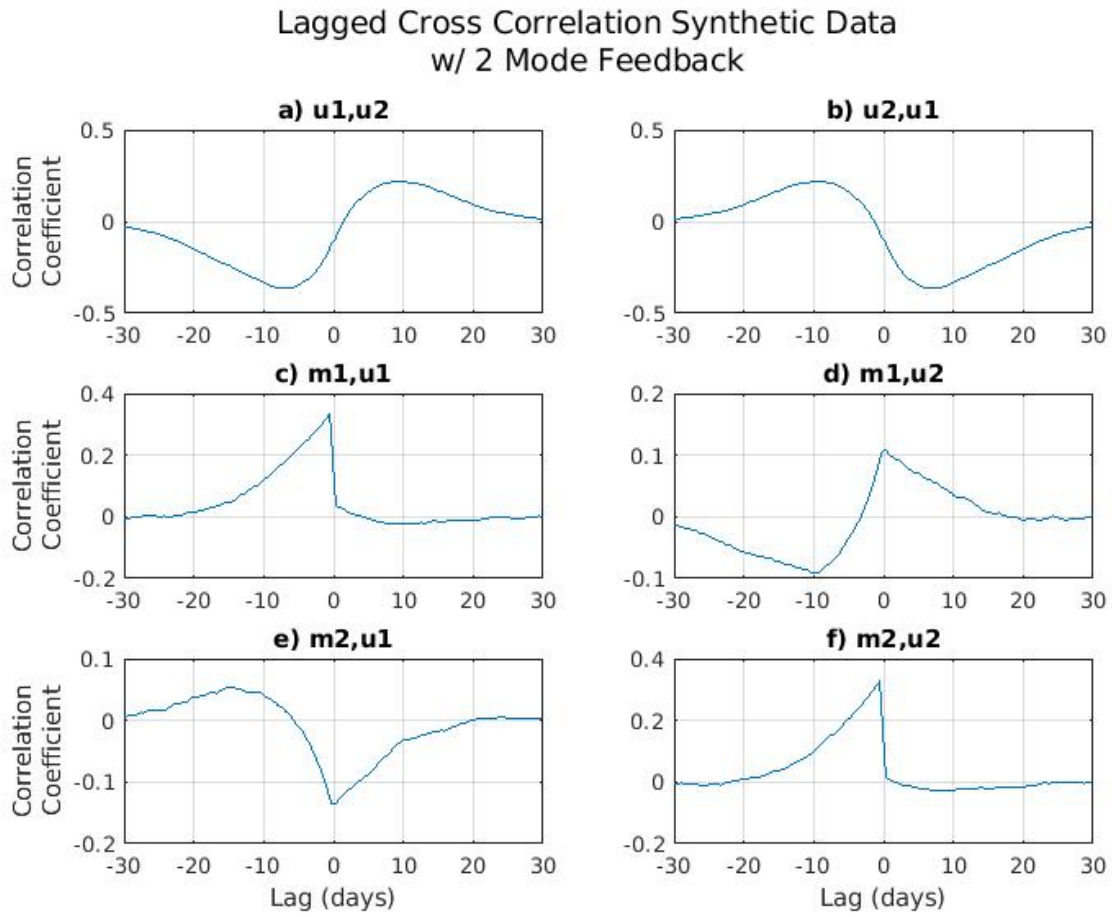

Figure 10. *Lagged Correlation analysis of Synthetic Data with two mode feedback. A) Cross correlation of u1u2 B) cross correlation of u2u1 C) Cross correlation of m1u1 D) Cross correlation of m1u2 E) cross correlation of m2u1 F) Cross correlation of m2u2.*

lags show when $u1$ leads $m1$. They show large positive correlations at short negative lags, which corresponds to the eddy momentum flux leading the zonal wind (Lorenz & Hartmann, 2001). However, the positive lags differ a bit from what we see in Lorenz and Hartmann (2001). We have small positive correlations at extremely short lags, followed by prolonged small negative correlations at higher lags. This would signify a feedback because we have nonzero correlations at large positive lags (7-21 days) for these cross correlations. But $m1u1$ and $m2u2$ are not the only cross correlations we are interested in as we can look at the cross correlations of one mode of u and the second mode of m and vice versa. We will focus on large positive lags (7-21 days) where saw the nonzero correlations $m1u1$ in and $m2u2$. In $m1u2$ we see positive correlations that decrease from lag = 0 to about lag = 20. In $m2u1$, we have negative correlations over the same lags. The fact that these correlations have opposite signs means that they likely work to cancel each other out to some degree. The $m2u1$ negative correlations at long lags are slightly large in magnitude than the $m1u2$ positive correlations. We can identify the feedbacks in the plots quite clearly and we can now look to quantify the feedback parameters. The feedback parameters we chose are shown in Table 1 and we hope to be able to accurately back them out in the next section.

3.1.2 Backing out Feedback Parameters

We see the effects of the feedbacks that we imposed on the data, but we can also now attempt to back out the feedback parameter for each pair. We can back out the feedback parameter in the one feedback case with a simple division of the covariances of u and m in the equation shown here.

$$a = \frac{cov(m)}{cov(u)} \qquad \textbf{Equation 10}$$

where a is the feedback parameter, $cov(m)$ is the covariance of m and $cov(u)$ is the covariance of u. This will give feedback parameters for each time lag, we can average over the time lags to get one value for the feedback.

Backing out the feedbacks in the two-mode feedback case is a little more complex. Eq. 3 shows that there will be 4 different feedback parameters in a two-mode feedback. If you expand Eq. 3, there will be a 2x2 matrix of feedback values, as seen in Table 1. Table 2 shows what the values of the imposed feedback parameters were when we created the dataset with the two-mode feedback.

$$\begin{pmatrix} cov(u_1u_1) & cov(u_2u_1) \\ cov(u_1u_2) & cov(u_2u_2) \end{pmatrix} * \begin{pmatrix} a_{11} \\ a_{12} \end{pmatrix} = \begin{matrix} cov(m_1u_1) \\ cov(m_1u_2) \end{matrix} \qquad \textbf{Equation 11}$$

$$\begin{pmatrix} cov(u_1u_1) & cov(u_2u_1) \\ cov(u_1u_2) & cov(u_2u_2) \end{pmatrix} * \begin{pmatrix} a_{21} \\ a_{22} \end{pmatrix} = \begin{matrix} cov(m_2u_1) \\ cov(m_2u_2) \end{matrix} \qquad \textbf{Equation 12}$$

The reason we have two sets of equations above is to emphasize the importance of the coupling vs uncoupling. We can see how using these two equations couples the two modes. We use Eqs. 11 and 12 to solve for the a terms, or feedback parameters in this equation. Like we did in Eq. 10 for solving the one mode feedback, we use the auto covariances of u along with the cross covariances of u and m to solve for each of the 4 feedback parameters. We should note here in the feedback calculation, we take the mean of the feedback parameters over the time lags of 10 to 20 days. We choose these values because we want to avoid the short-term feedback effects while also avoiding the really long lags (20+) where the damping takes over.

In Table 2, we see the actual feedback parameters that we imposed along with the feedback parameters that we backed out using Eqs. 11 and 12. We found that using our equations to back out the feedback parameters, we were able to very closely duplicate the feedback parameter that we used in the generation of the dataset. We hope to use this ability to

find the feedback parameters in the reanalysis data.

	a11	a12	a21	a22
Imposed Feedbacks	0.0417	0.0833	-0.0833	0
Backed out Feedbacks	0.0404	0.083	-0.0871	-0.0141

Table 2*. Imposed and Backed out Feedback Parameters.*

3.2 ERA-Interim Data

The synthetic dataset gives us an easy and simple way to control the feedbacks and see how the feedback parameters affect the zonal mean wind and the eddy momentum flux while gaining significant insight about the changes in variability between the no feedback and the feedback cases. Now, we will attempt to reproduce our analysis of the synthetic data with ERA-Interim data. Before diving into some seasonal analysis, we will first work with all our data as a one full dataset (From January 1 1979 to December 31 2017). Once we see that our analysis works for the full dataset, we can break it down further into seasons to identify more specific variability changes. If we solely look at the full dataset, the feedbacks may not show up as clearly as they would in each season. If we have a positive feedback in one season and a negative feedback in a different season, those may cancel out and appear as no feedback in the full data. But, using the full data first will give us a general understanding of how the feedbacks show up in correlations and if we can quantify them using our method from the previous section.

The first thing that we can do with our full reanalysis data is plot both EOF 1 and EOF 2 in the same manner that we did with the model data and synthetic data. However, for the reanalysis data, we will split the data into hemispheres because as we mentioned earlier, it tends to be easier to see the results in the Southern Hemisphere. We can then further break this down

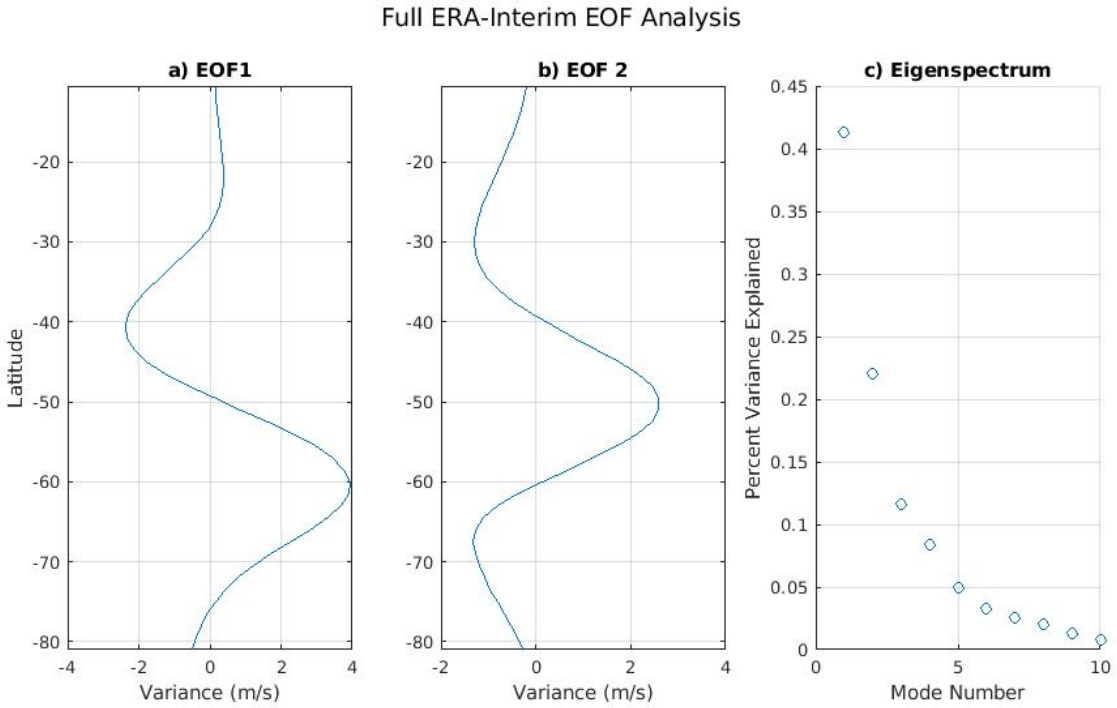

Figure 11. *Full ERA-Interim EOF Analysis showing a) EOF1 b) EOF2 and c) the Eigenspectrum which shows how much variance is explained.*

into seasons. In Fig. 11, we show EOF1 and EOF2 for the full ERA-Interim data to get a sense for the orientation and shape of the EOFs before we begin analyzing the seasonal data. The center of the Southern Hemisphere jet is between 40°S and 60°S and peaks at about 50°S which is shown in Fig. 5 and also corroborated here in Fig. 11. EOF 1 shows peaks in the variance to the north and south of the jet center while EOF 2 shows the peak variance right near the center of the jet. The eigenspectrum shows that EOF 1 of the Southern Hemisphere explains nearly 42% of the variance while EOF 2 explains about 22% in the reanalysis data. In the future, we could apply all of the steps we took to look at the Southern Hemisphere and simply change them to

look at Northern Hemisphere. We could get some insight into the jet behavior in the Northern Hemisphere as we did in the Southern Hemisphere, but for now, the focus is solely on the Southern Hemisphere. Now that we have a good understanding of the EOF structure in the zonal-mean wind, we can now dive deeper into how the zonal mean wind and eddy momentum flux interact and how they affect the variability in the jet stream.

3.2.1 Going from Principal Components to Correlations

There is a conversion that takes place to get from the principal components that we get from the EOF analysis to ultimately get the auto and cross correlations. In Section 2.4.4, we step through how we get the principal components for u and m. Once we have the PCs, we calculate the power spectrum of the data. We can do this using each combination of u and m for both modes. Once we have the power spectra, we can convert to covariance. To see how this is done, see the Appendix. There is a simple conversion from covariance to correlation that leaves us with the necessary correlations for analysis.

3.2.2 Lagged Correlation Analysis

We will first look at the full dataset to introduce and analyze the correlations. The correlations we will focus on are shown in Fig. 12 and there is a lot to investigate here. We notice in Figs. 12a and 12b how the $u1$ and $u2$ auto correlations look similar to the auto correlations we saw in the synthetic data. The $u1$ and $u2$ correlations approach zero near lag = ±30 days. How these auto-correlations and ultimately the persistence of u1 and u2 change with feedbacks vs no feedbacks will be discussed later.

If we look at Fig. 12c correlations, we see positive correlations at large positive lags for $u1u2$. The positive correlations at positive lags in $u1u2$ and negative correlations at negative lags implies a propagation of the zonal mean zonal wind. The implication here of propagation paired with the orientation of the EOFs shows a poleward propagation. When the cross correlation of $u1$ and $u2$ produces a positive correlation, and knowing that $u1$ leads $u2$, we can

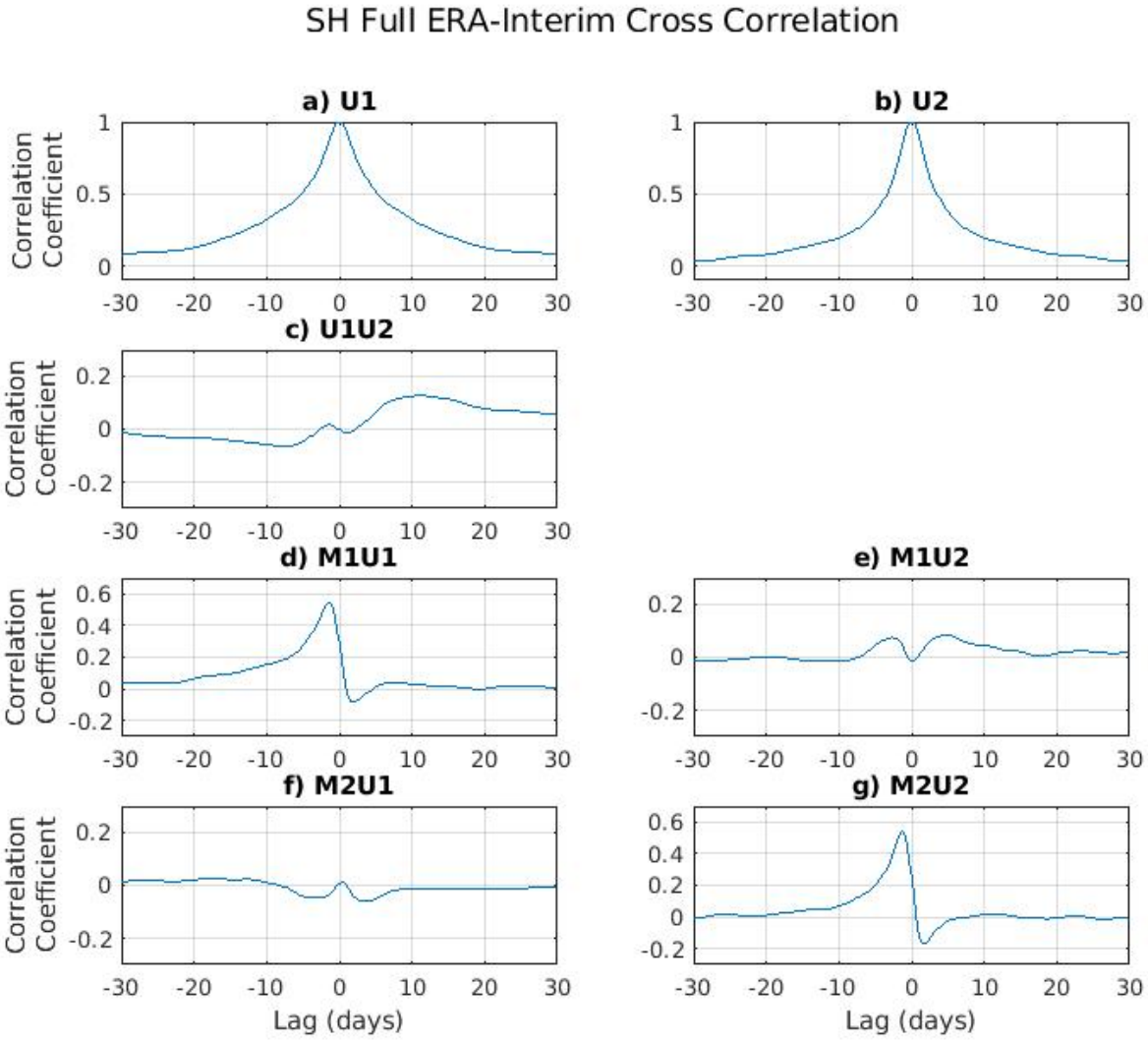

Figure 12. *ERA-Interim full data lagged correlation analysis. A) Auto correlation of u1 B) Auto correlation of u2 C) Cross correlation of u1u2 D) Cross correlation of m1u1 E) Cross correlation of m1u2 F) Cross correlation of m2u1 G) Cross Correlation of m2u2.*

deduce the implication of poleward propagation. We could also look at the correlations of $u2u1$

but we see that the correlations are the exact opposite of $u1u2$ so there is no need to investigate this one individually. We are simply changing the order of the $u1$ and $u2$ which only changes the sign of the correlations, while leaving the magnitudes identical.

In Fig. 12d, we notice that the shape and the magnitude of the $m1u1$ plot is similar to the corresponding plot in Lorenz and Hartmann (2001, see Fig. 5). In our plot, we see that at long positive lags (7-21 days), there is a positive correlation. We also see that at short positive lags, there are negative correlations. This does not mean there is a negative feedback necessarily at short lags, but could be caused by the negative autocorrelations in the eddy momentum flux anomalies (Lorenz and Hartmann, 2001). We will not focus on the nonzero correlations at short lags in this study, but it is something that should be investigated further in future research. Instead, we will focus on the long-term correlations that effect the low frequency variability of u. In the $m2u2$ (Fig. 12g) plot, we see a similar pattern, but the positive correlations at large lags are less pronounced and much closer to zero. However, the negative correlations at short positive lags are more negative making this feature more pronounced. This is one benefit of using the two-mode feedback as we are able to pick up on some of these subtle differences.

We just investigated the cross correlations of u and m from the same mode, but we can gain insight by looking at some other cross correlations of u and m from opposite modes, like $m1u2$ and $m2u1$. In the $m1u2$ plot, we see positive correlations at large positive lags. The positive correlations here mean $u2$ leads $m1$. In the $m2u1$ plot, we see negative correlations at large positive lags. With negative correlations, the feedback at large positive lags is also negative. For there to be propagation, the feedbacks must have opposite signs. Depending on which one is positive, the propagation will be either poleward or equatorward. Because we have positive a12 and we saw that $u1$ leads $u2$, we can infer poleward propagation. This is why when

we impose our feedbacks in the synthetic data, we use opposite signs for *a12* and *a21*. We will see later that the backed-out feedback parameters are also opposite in sign.

When we compare the correlations of the full year data and the synthetic data, we see similar correlations along with some key differences. First, the full year data has more noise present than the synthetic data, as expected. However, the noise is not significant enough to interrupt our analysis moving forward. The $u1u2$ cross correlations in the full year data and the synthetic data are both negative at large negative lags and positive at large positive lags. As mentioned earlier, this implies a propagation of the u wind. We see important difference between the full year data and the synthetic data at small lags. There is a slight change of sign at short positive and short negative lags. For this analysis, we will not investigate this potential low frequency feedback, but further insight could be gained by doing so.

In the cross correlations of u and m, we notice again that there is a potential low frequency feedback at low lags. We will focus on what is happening at greater lags. At large positive lags in the full year data, we see positive correlations for $m1u1$, and near zero correlations at $m2u2$. This could signify a feedback in the mode one but not one in mode 2. In the synthetic data, we see a negative correlation at large positive lags for both $m1u1$ and $m2u2$. Although the correlations are negative, because they are nonzero in the synthetic data, there is a feedback implied in both modes. When we look at the $m1u2$ correlations for the full data, we see positive correlations at large positive lags which again signifies that a feedback is present. This is in agreement with the synthetic data correlations of $m1u2$ and we see similar agreement in $m2u1$. We can now work to quantify the feedback parameters since we have proven there are feedbacks in the data.

3.2.3 Finding feedbacks to solve for zero feedback case

After analyzing the actual reanalysis lagged correlations, we can use the same technique we found using the synthetic data to back out the feedback parameters. Once we have the feedback parameters, we can solve for a case where we take out the feedbacks and see what the results would be on not only the correlations, but also the impact the feedbacks have on the variability.

To back out the feedback parameters, we will be using Eqs. 11 and 12 like we did to solve the feedback parameters for the synthetic data. In Table 3, we see the four backed out feedback parameters for the full year of data. In a later section, we will break down the data into seasons. We note that there is a positive feedback for a11. We would expect this to be the case because previous studies have shown a feedback when looking at only the first mode (Lorenz & Hartmann, 2001). It is important to note the signs of a12 and a21. The signs of these two feedbacks are opposite in sign with a12 having greater magnitude. When a12 is positive and a21 is negative, we understand that will produce poleward propagation. Also, the greatest feedback for the full ERA-Interim data is a12 and we will see if this is the case over the other seasons.

	a11	**a12**	**a21**	**a22**
Full ERA-Interim Feedbacks	0.0432	0.0665	-0.0215	0.0402

Table 3. *Full Data backed-out Feedback Parameters.*

Once we have the feedbacks quantified, we can remove the effect of the feedbacks on the observed lagged covariances and correlations to quantify their effect on the u variability. Recall that to calculate the lagged covariances we first calculated power spectra and then used properties of Fourier transforms to get covariances. The reasons for this choice will become

clear below. To get the power spectra for the zero-feedback case, we begin by using the original principal components from the feedback case and use the feedbacks we just found to create principal components for the zero-feedback case. We use Eqs. 13 and 14 below to create the zero feedback principal components for the eddy momentum flux convergence:

$$\tilde{m}1 = m1 - (a11 * u1) - (a12 * u2) \quad \textbf{Equation 13}$$

$$\tilde{m}2 = m2 - (a21 * u1) - (a22 * u2) \quad \textbf{Equation 14}$$

where $\tilde{\mathrm{m}}1$ and $\tilde{\mathrm{m}}2$ are the zero-feedback eddy momentum flux PCs of mode 1 and mode 2, respectively.

Once we have $\tilde{\mathrm{m}}1$ and $\tilde{\mathrm{m}}2$ we can calculate the auto power spectra for the eddy momentum flux convergence terms. To calculate the relationships between u and m under no feedbacks, it is easiest to work in Fourier transform space because the inter-variable relationships involve algebra instead of calculus. Let M_1 denote the Fourier transform of m_1. Note that M_1 is a function of frequency (ω) and m_1 is a function of time (t). By definition, the power spectrum of m_j is $M_j M_j^*$ where the asterisk stands for the complex conjugate. To determine the other variables from the $\tilde{\mathrm{m}}$ calculated above, we first use the momentum budget equation:

$$c_j \frac{du}{dt} = m_j - \frac{u_j}{\tau_j} \quad \textbf{Equation 15}$$

where we add a constant c, which is close to one, to account for the neglect of several small terms in the momentum budget and j represents the mode number (ie. EOF1 or EOF2). Transforming Eq. 15 to Fourier space, we get:

$$ic_j \omega U_j + \frac{U_j}{\tau_j} = M_j \quad \textbf{Equation 16}$$

where i is imaginary and ω is frequency and we use the fact that the Fourier transform of the time derivative of u is $i\omega U$. Multiplying the above equation by U* and rearranging:

$$\left(\frac{1}{\tau_j} + ic_j\omega\right) = \frac{M_j U_j^*}{U_j U_j^*} \qquad \textbf{Equation 17}$$

where, by definition $M_j U_j^*$ us the M_j and U_j cross spectrum and $U_j U_j^*$ is the U_j power spectrum. Looking at the ratio of $M_j U_j^*$ to $U_j U_j^*$ (not shown), we do in fact see that the real part is a constant and the imaginary part increases linearly with frequency just as predicted from Eq. 17. This relationship is the most robust at low frequencies probably because U variability is very weak at high frequencies. A similar equation results from multiplying Eq. 16 by M*:

$$\left(\frac{1}{\tau_j} + ic_j\omega\right) = \frac{M_j M_j^*}{U_j M_j^*} \qquad \textbf{Equation 18}$$

This equation has the same left-hand side as Eq. 17. The above discussion suggests that the constants τ and *c* can be determined from the ratio of $M_j U_j^*$ to $U_j U_j^*$ or $M_j M_j^*$ to $U_j M_j^*$ at low frequencies. Here we use both by averaging the right-hand sides together and then defining 1/τ and *c* as that which minimize the squared error in two equations over frequencies less than 0.05 day^{-1}.

To find the *m* and *u* with no feedback we assume the constants *c* and τ are unchanged and therefore Eq. 16 still holds. Multiplying by $\widetilde{M}_k^*$, we find the relationship between the M and U cross spectrum with no feedback:

$$\widetilde{U}_j \widetilde{M}_k^* = \frac{\widetilde{M}_j \widetilde{M}_k^*}{\frac{1}{\tau_j} + ic_j\omega} \qquad \textbf{Equation 19}$$

where *j* and *k* are both a mode (ie. EOF1 or EOF2). They might be the same mode, but we are also looking at cross mode relationships so *j* and *k* could be different modes. Similarly, multiplying each side of Eq. 16 by the conjugate of itself gives:

$$\widetilde{U}_j \widetilde{M}_k^* = \frac{\widetilde{M}_j \widetilde{M}_k^*}{\frac{\frac{1}{\tau_j}+ic_j\omega}{\frac{1}{\tau_k}+ic_k\omega}}$$ **Equation 20**

Using these 2 equations we can calculate all combinations of the U and M and U and U cross and power spectra from the M cross and power spectra. We then use a Fourier transform to convert these calculated spectra to cross covariances and correlations as discussed previously.

3.2.4 Feedback impact on Variability

With one case of actual full reanalysis data and one case with the feedbacks removed, we can use some simple statistics to see what affect the feedbacks have on the variability of the system, especially the effects on the zonal wind and eddy momentum flux. We can solve for how much of the actual variance is contained in the no feedback case by taking the covariance at lag = 0 of the no feedback U and divide by the actual case.

It should be noted that we will take the 30-day running mean of the lagged covariances due to the timescale of the annular mode. The annular mode is typically defined on monthly time scales, therefore, it is most relevant to compare the effect of the feedbacks on the variance at monthly time scales. The variance of the monthly-mean can be calculated from the 6-hourly auto covariance as follows. Let $p(t)$ be a time series and $c(s)$ be the auto covariance of p at lag s:

$$c(s) = \frac{1}{T}\sum_{t=1}^{T} p(t+s)p(t)$$ **Equation 21**

where T is the number of times in the record. Define $\hat{p}$ to be the 2n+1 running mean of p:

$$\widehat{p(t)} = \frac{1}{2n+1}\sum_{i=-n}^{j=n} p(t+j)$$ **Equation 22**

The auto covariance of $\hat{p}$ after distributing the sums is:

$$\widehat{c(s)} = \frac{1}{T(2n+1)^2}\sum_{t=1}^{T}\sum_{k=-n}^{n}\sum_{j=-n}^{n} p(t+j)p(t+s+k) \qquad \textbf{Equation 23}$$

Switching the order of the sums so that the t sum is performed first and using the definition of auto covariance (i.e. $c(s)$), we get:

$$\widehat{c(s)} = \frac{1}{(2n+1)^2}\sum_{k=-n}^{n}\sum_{j=-n}^{n} c(s+k-j) \qquad \textbf{Equation 24}$$

Let $l = k - j$. Counting the number of times $c(s+l)$ is repeatedly summed for each value of l finally leads to

$$\widehat{c(s)} = \frac{1}{(2n+1)^2}\sum_{l=-2n}^{2n}(2n+1-|l|)c(s+l) \qquad \textbf{Equation 25}$$

Using this equation for lag 0 (i.e. $s = 0$), we can compute the variance of the $2n+1$ running-mean of p from the auto covariance of the 6 hourly p. To estimate the change in the monthly mean variance we choose n to be 60, which translates to a thirty day plus 6 hour running mean.

For EOF 1, the change of variance in the 30-day running mean case (which we will use from here on out), the no feedback case accounts for 56% of the feedback in the actual case. This is more easily understood by saying that the removed feedbacks account for 44% of the variance. For EOF 2, the feedbacks account for about 36%. As we see in EOF 1, the feedbacks account for a large amount of variance and if we break the full data into seasons, we can see if the feedbacks have more of an effect in certain seasons. The analysis up until now has focused on the full ERA-Interim data. We now have an understanding for what the full year EOFs and correlations look like. We also stepped through how to calculate the change of variance, using values from the full ERA-Interim data. Going through these steps gives us an idea of the features to look for in the analysis and shows us how to calculate the change of variance. In the

next section, we will look at our data in 4 different seasons (DJF, MAM, JJA, SON) to assess the seasonality of the feedbacks.

3.2.5 Seasonal Analysis

Before we dive into the lagged correlation analysis of the individual seasons, we should take a quick look at the plot of EOFs for each of the seasons to make sure they agree with our understanding of EOF analysis since we will be use the PCs of the EOFs in our analysis. In Fig. 13, we see the plots of both EOF 1 and EOF 2, along with the eigenspectrum for each season of our ERA-interim data. We note that EOF1 shows the leading mode of variability to be the north-south fluctuation of the jet when pairing the orientation of the EOFs in Fig. 13 to the mean state (Fig. 5, also Fig. 14). We see that in Fig. 13a, there are maximum values poleward of the center of the jet and negative values equatorward of the jet, emphasizing

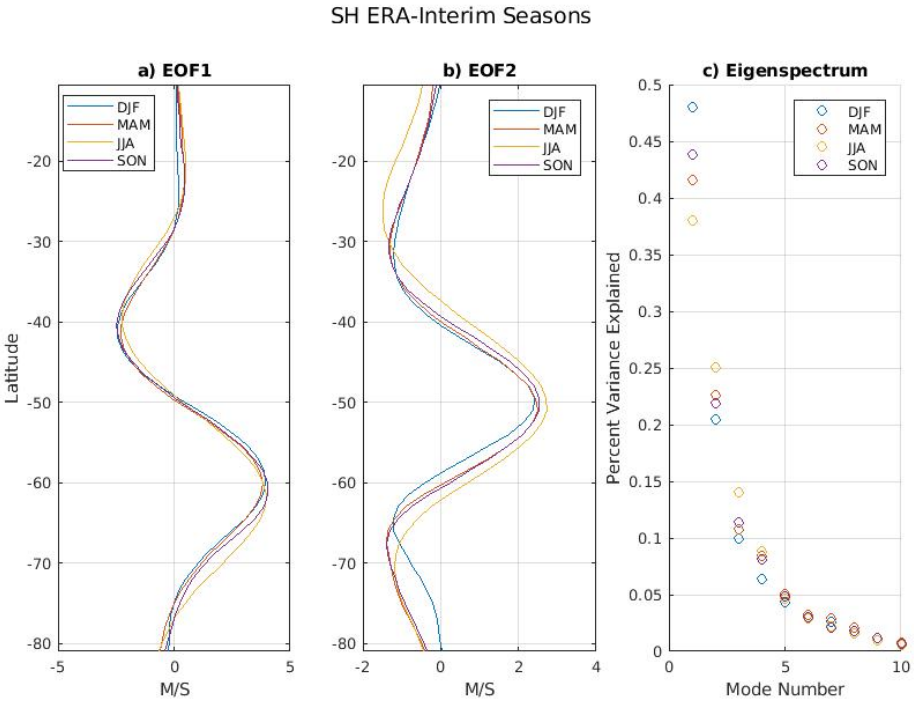

Figure 13. *ERA-Interim EOF analysis divided into seasons showing a) EOF1 b) EOF2 and c) the Eigenspectrum.*

the fact that EOF 1 explains the most variance in the north-south variability of the jet. EOF2 shows the second mode of variability which is the strengthening and sharpening of the jet. We see this with maximum values in Fig. 13b near the center of the jet and minimum values on both the poleward and equatorward side of the jet center. In Fig. 13c, the eigenspectrum shows the percent variance explained by each mode. We see clearly that EOF1 explains the most variance and explains about twice as much variance as EOF2. After EOF2, the percent variance explained gets really small and we will ignore these modes for now.

An interesting side point to note here is how well in agreement EOF1 and EOF2 are. If we look at the zonal wind atmospheric cross sections, we will see that there tends to be large variance in the shape and strength of the jet from season to season or even month to month. We see the cross sections of monthly mean zonally

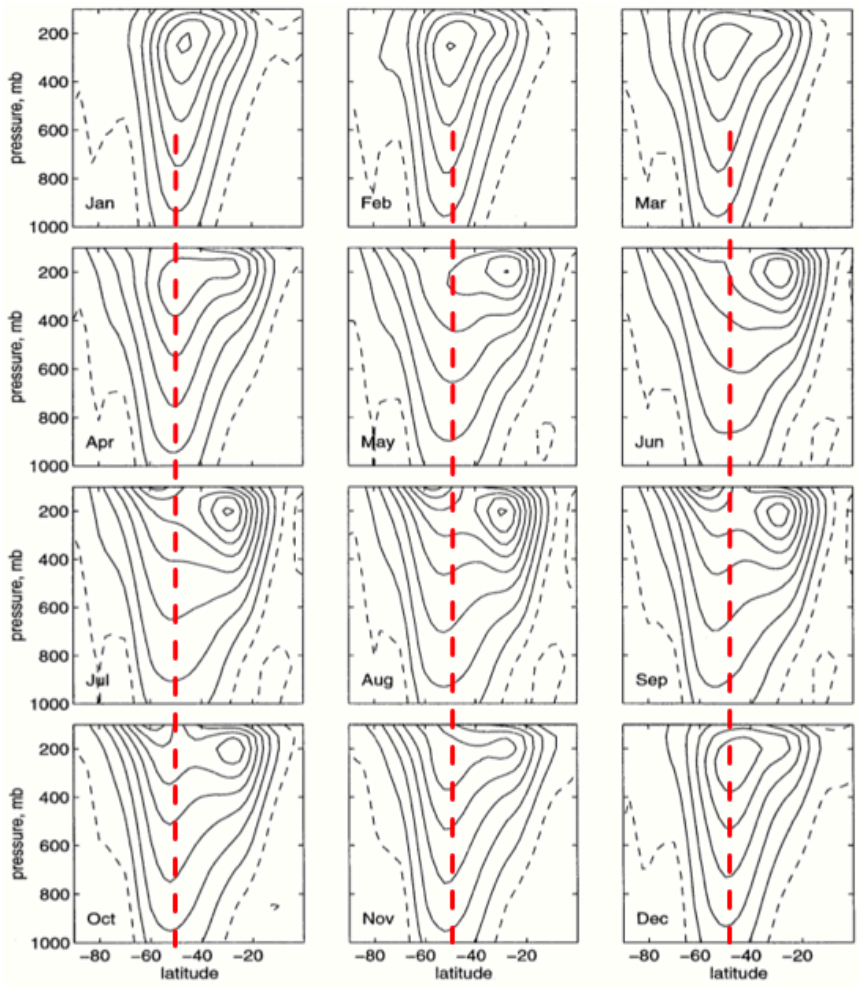

Figure 14. *Fig.1 from Hartmann and Lo (1998) showing the monthly mean zonally average zonal wind from 1985-1994 with a contour interval of 5 ms^{-1}. The zero and negative contours are dashed and the red dashed line denotes the 50°S center of jet.*

average zonal wind in Fig. 14 which is from Hartmann and Lo (1998). They take the monthly mean from 1985-1994 and plot the zonally average zonal wind in a latitude vs pressure plot. We see how much variation there is from season to season, especially in the upper levels and where the jet strength peaks. However, the EOF analysis does not show much seasonal variability even though we see how much variation is in the month to month plots shown here (Hartmann & Lo, 1998). However, we added a dashed red line to show the center of the midlatitude jet and the location of the midlatitude jet is remarkably consistent and the strength is fairly consistent as well. Also, because the midlatitude jet dominates here at lower levels, the EOF analysis that we did picks up on the midlatitude jet variability and shows great seasonal consistency.

For each season, we will also attempt to go through the same process laid out above with the exception that we will also add an uncoupled case to emphasize the importance of a coupled feedback.

3.2.5.1 Lagged Correlation Analysis (JJA)

The previous steps included work with a full set of our data but now we will work with the seasonal data. The first season we will analyze is the Southern Hemisphere winter of June-July-August (JJA) because the results are more well defined and explaining them first will provide a general understanding of the seasonal analysis for the rest of the seasons. Table 4

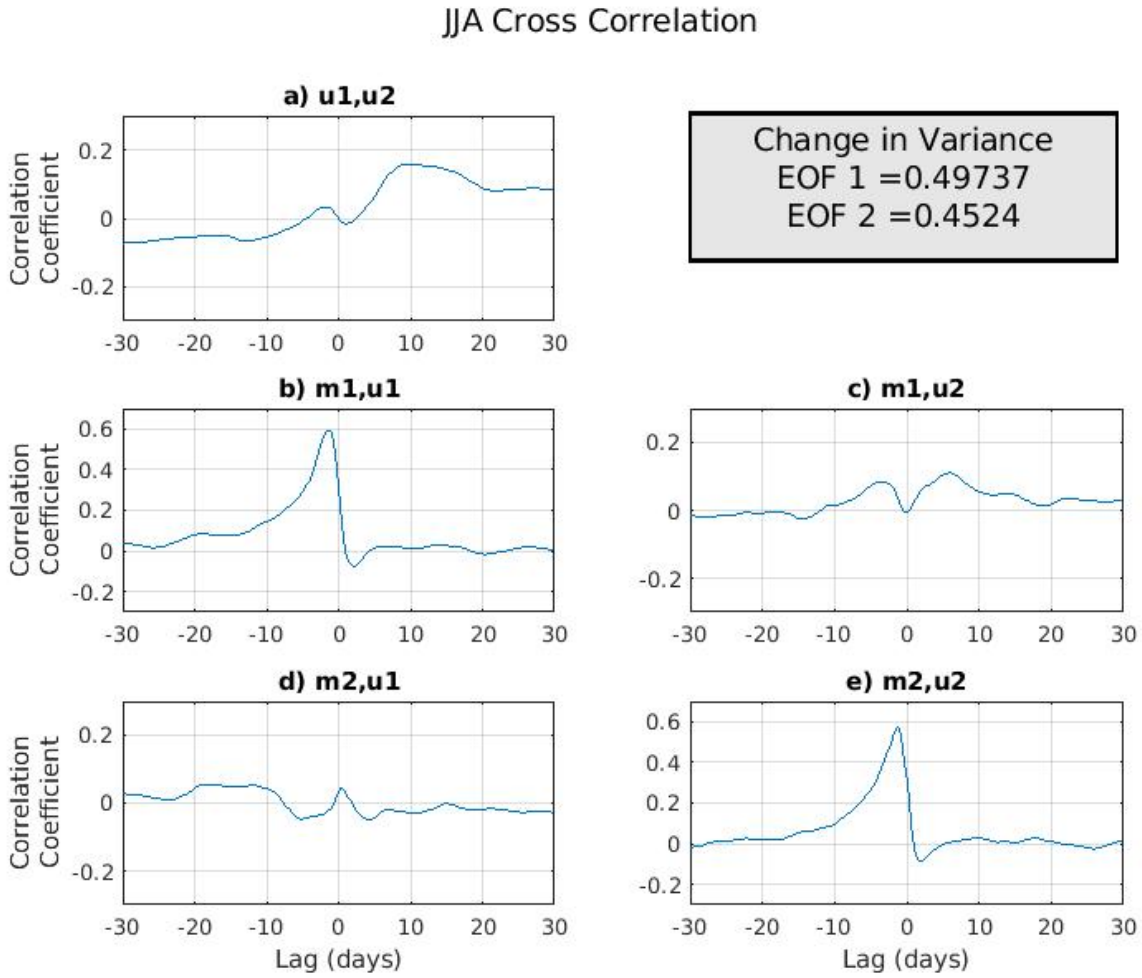

Figure 15. *Lagged Correlation analysis for JJA. A) cross correlation of u1u2 B) Cross correlation of m1u1 C) Cross correlation of m1u2 D) Cross correlation of m2u1 E) Cross correlation of m2u2. Change of Variance for 30-Day running mean also shown for both modes*

shows all of the feedback parameters for each of the seasons in our analysis.

In Fig. 15, we see correlations similar to the ones we saw for the full data, but there are some slight differences. In the JJA, we can note a couple of important features. In Fig. 15a, we

see the cross correlation of $u1$ and $u2$. We mentioned earlier that the positive correlations at long positive lags signifies a poleward propagation of the zonal wind. Also, the structure of EOF1 and EOF2 emphasize this poleward propagation in $u1$ and $u2$. It means that positive EOF2 leads to positive EOF1, which in Fig. 13 denotes a poleward shift from positive EOF2 around 50°S to positive EOF1 around 60°S. In the cross correlations of the *u* and *m* terms of different modes, we note some nonzero correlations at long lags. While the correlations at long lags in *m1u1* and *m2u2* may appear to be small, they are statistically significant and provide

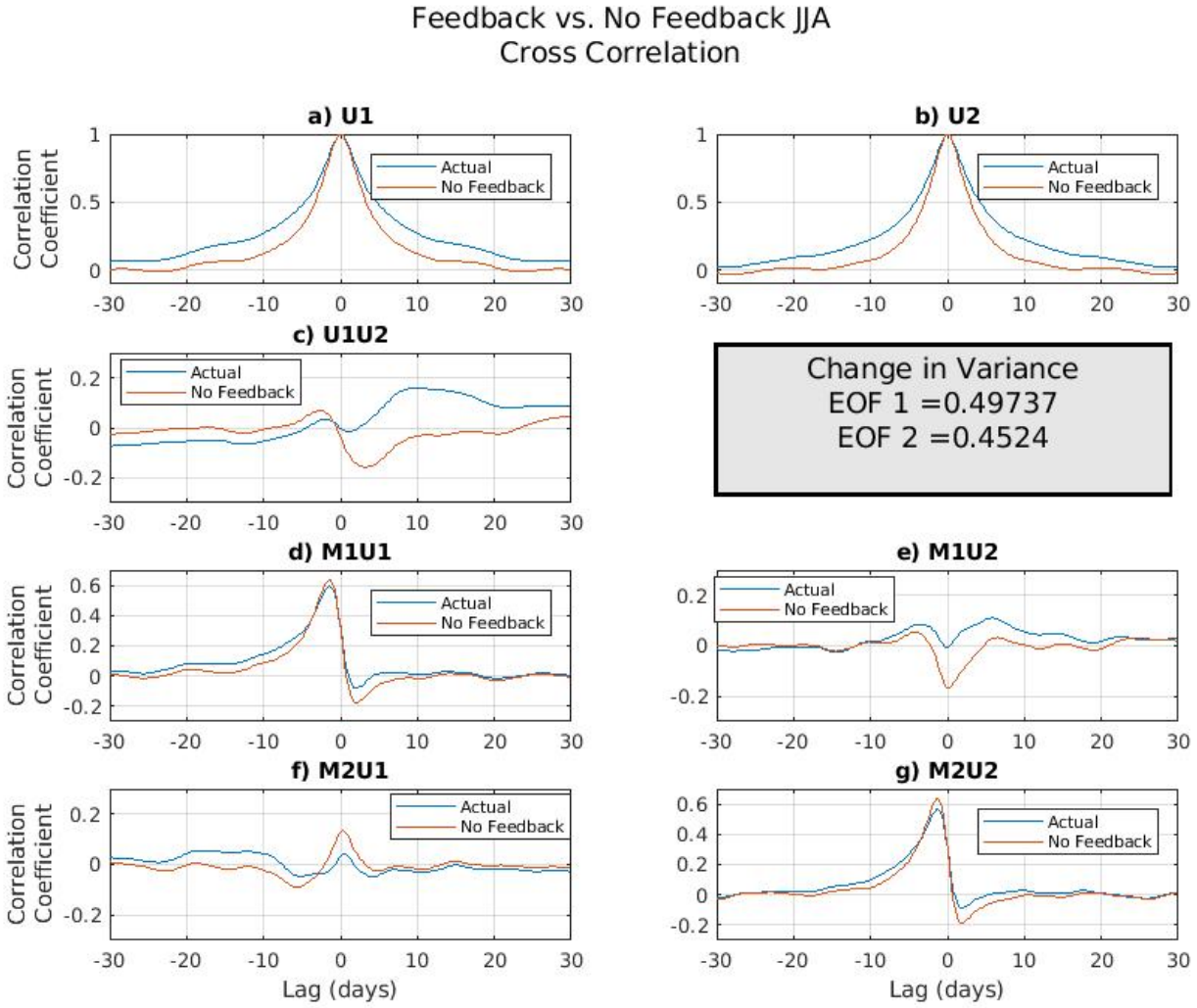

Figure 16. *JJA Lagged Correlation analysis for actual (blue) and no feedback case (red). A) Auto correlation of U1 B) Auto correlation of U2 C) Cross correlation of U1U2 D) Cross Correlation of M1U1 E) Cross correlation of M1U2 F) Cross correlation of M2U1 G) Cross Correlation of M2U2. Change of Variance for 30-Day running mean also shown for both modes.*

information about the complex nature of these feedbacks. We also see positive correlations of *m1u2* at long positive lags which are relatively high compared to the other cross correlations of *u* and *m*. Interestingly, the cross correlations for *m2u1* are slightly negative. The fact that *m1u2* and *m2u1* are opposite in sign is also a sign of poleward propagation. If the feedback parameters of those two relationships are opposite in sign, we can denote poleward propagation. Now that we have a general understanding of the actual correlations for JJA, we can compare the actual case to the no feedback case.

Fig. 16 shows the actual JJA (blue) and the case where we have removed the feedbacks (red). We can easily compare the difference in correlations due to feedbacks using this figure. In Figs. 16a and 16b, we note how the persistence in zonal mean changes when the feedbacks are removed. The correlations in the no feedback case drop lower than the actual case which we would expect because by removing the feedbacks, we are reducing the memory in zonal mean for both modes because a11 and a22 are positive. We can attribute this change in persistence directly to the feedbacks as those are the only difference between the two plots of data. The $U1U2$ is near zero for long positive lags when the feedbacks are removed. The difference at

	a11	**a12**	**a21**	**a22**
DJF Feedbacks	0.0291	0.0873	-0.0396	0.0076
MAM Feedbacks	0.0324	0.1153	-0.0243	0.0593
JJA Feedbacks	0.045	0.1138	-0.0228	0.0782
SON Feedbacks	0.0665	0.1156	-0.0383	0.0222

Table 4. *Feedback Parameters in* $days^{-1}$ *for ERA-Interim Seasonal Analysis.*

long positive lags between the actual and no feedback case is the largest amongst all of the cross correlations for JJA. This would signify that the feedbacks play an important role on the propagation of the zonal mean zonal wind. In Fig. 16d, we see the $M1U1$ correlation which is initially small but positive at larger lags become nearly zero or even slightly negative at those same lags. Again, as we noted in our synthetic data, by removing the feedbacks, the correlations at long positive lags should be at or near zero because *M* forces *U* but not the other way around in the absence of feedbacks. In figure 16g, the $M2U2$ correlation is also lower (more negative) in the no feedback case and stays slightly negative until about lag = 10days. Figure 16e shows a fairly significant difference in the actual and no feedback. The actual correlation for JJA $M1U2$ shows the largest positive correlation across the four combinations of zonal mean wind and eddy momentum flux cross correlations for both modes. The correlation at lag = 7 days is 0.1 or slightly greater which is much higher than the other cross correlations at that point. Also, it stays positive until about lag = 21 days showing significant persistence of this feedback. This correlation signifies that EOF2 of u leads to eddies that force EOF1. When the feedback is removed, the correlation drops quickly to zero after being slightly positive at lag =7 days. The difference between the actual case and the no feedback case is the greatest at the lags (7-21days) we are focusing on to identify and quantify feedbacks. This is in agreement with the highest feedback parameter for JJA which is a12 = 0.1138 day^{-1}. In Fig. 16f, we see the $M2U1$ correlation at large lags is slightly negative nearly identical in the actual data compared to the no feedback case. We see the feedback parameter for a21 in JJA is -0.0228 day^{-1} which is very small compared to a12. While the feedback parameters line up with what we see in the plots, we cannot make too many conclusions about the strength and the exact effect between the different relationships. Due to the complex nature of the system, the net effect of a large a12 is not

necessarily intuitive on the coupled EOF1/EOF2, therefore below we must explicitly calculate the effect of these feedback parameters on the *u* variability in order to understand how they affect the variance and the persistence.

In Fig. 16, we also show the change in variance for EOF 1 and EOF 2 between the actual reanalysis data and the no feedback case. The change of variance calculation divides the covariance of the no feedback case by the covariance of the actual case at lag = 0. If the change in variance is below 1, the feedbacks add, or account for, variance and if the variance is above 1,

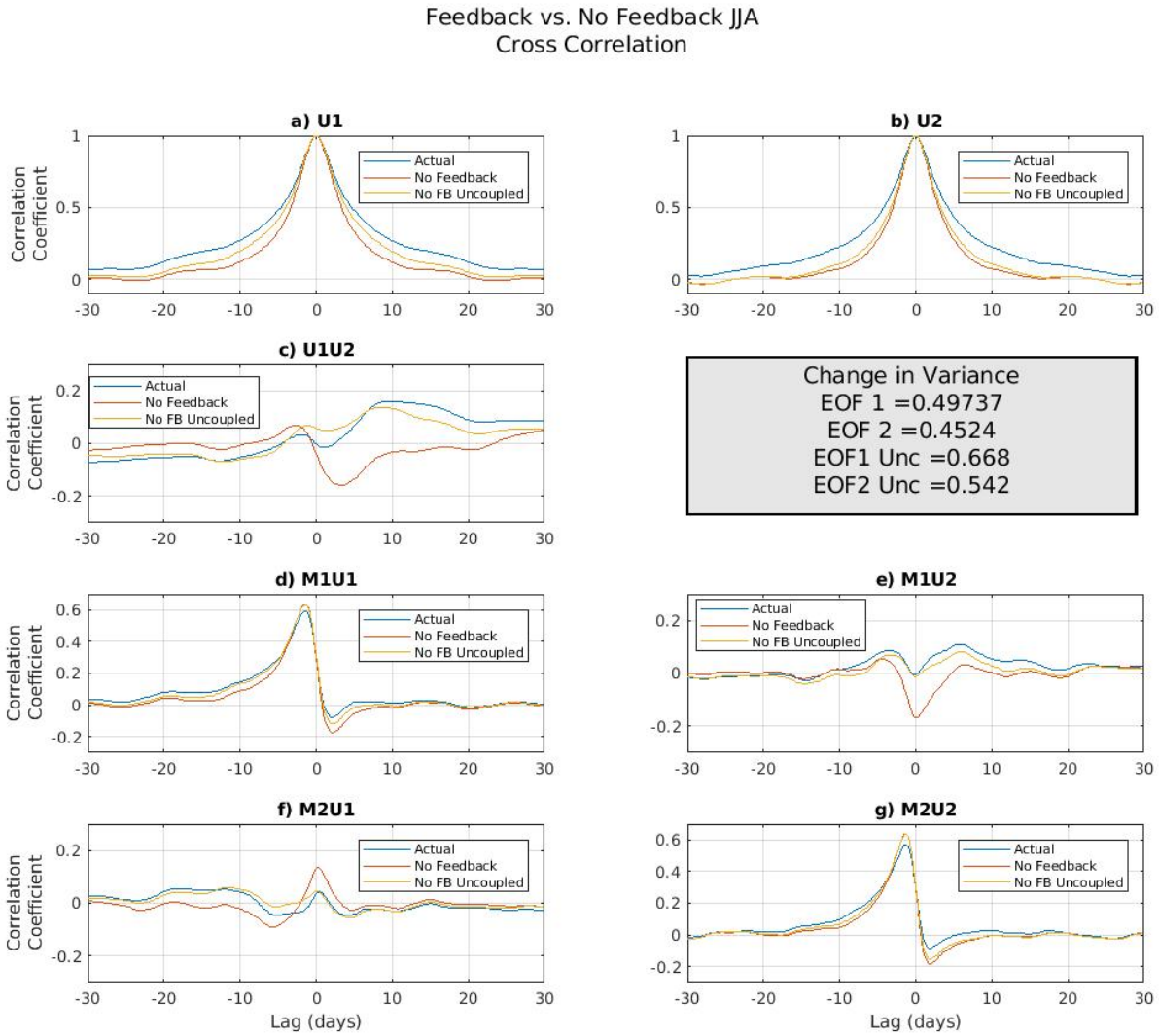

Figure 17*. JJA Lagged Correlation analysis for actual coupled (blue), coupled no feedback case (red) and uncoupled no feedback case (yellow). A) Auto correlation of U1 B) Auto correlation of U2 C) Cross correlation of U1U2 D) Cross Correlation of M1U1 E) Cross correlation of M1U2 F) Cross correlation of M2U1 G) Cross Correlation of M2U2.Change of Variance for 30-day running mean also shown for both modes.*

then the feedbacks reduce the variance. We see that the change in variance for 30-day running mean of EOF 1 is 0.497, which means that the feedbacks for mode 1 account for about 50% variance. For EOF 2, the change in variance is 0.452, which means that the feedbacks add about 55% variance. These numbers are significant and emphasize the importance of identifying and quantifying these feedbacks. The feedbacks account for a significant portion of the variance in the zonal mean zonal wind and by better understanding and quantifying these feedback parameters, we should be able to better understand the variability in the jet and where it comes from.

As we mentioned earlier, past studies only looked at one mode of the variability without coupling. Recall that when we say coupled, we mean that EOF1 and EOF2 interact and uncoupled means they are assumed to be completely independent. To investigate the importance of using two coupled modes of variability, we decided to do the exact same analysis, except we remove the coupling feedbacks (set a12 and a21 to zero, see Appendix for more) and see how the lagged correlation analysis and the change in variance are affected. In Fig. 17, we take a look at how the JJA plots compare when we only use 1 mode and ultimately uncouple the data across the modes. Fig. 17 shows all of our JJA plots together where we have the actual case (blue), the no feedback coupled case (red), and the no feedback uncoupled case (yellow) for easy comparison. In Figs. 17a and 17b, we see a reduced effect of removing the feedbacks when the system is uncoupled on persistence. The persistence of both $U1$ and $U2$ is less reduced when the feedbacks are uncoupled. However, the no feedback uncoupled case has higher persistence than the no feedback coupled case which means there is some feedback occurring in the uncoupled case that should not be. The sign of this feedback matters for persistence. Again, if we remove the feedbacks in a coupled and uncoupled system, we would expect the resulting correlations

would be almost identical but they are not. This emphasizes that something else is going on in an uncoupled system that we do not quite understand and is reason for why it is important to use a coupled feedback system. We see a big change in the $U1U2$ correlation in figure 17c between the two no feedback cases. In the coupled no feedback case, the correlations become nearly zero at long positive lags. However, in the no feedback uncoupled case, the correlations are almost the same as the actual coupled correlations. This does not make sense intuitively because as we mentioned earlier, the $U1U2$ positive correlations at these long lags signifies poleward propagation. In the coupled no feedback case, these positive correlations disappear and it would stand to reason that the poleward propagation of the zonal mean zonal wind is caused or influenced by these feedbacks. But the uncoupled no feedback case positive correlations seem to show that this poleward propagation still persists even when the feedbacks, which are supposedly a driver for this poleward propagation (Feldstein S. B., 1998), are removed. Again, this shows how important the coupling is when trying to diagnose these feedbacks. In the *U* and *M,* cross correlations, we find that the uncoupled no feedback case tends to fall in between the correlations of the actual and the no feedback coupled case. What this means is that the uncoupled case does not show as drastic of an effect of the removal of feedbacks as the coupled case. There is still a slight shift towards lower magnitude correlations at long positive lags in the $M1U1$ and $M2U2$ no feedback uncoupled correlations compared the coupled no feedback case. The change between the actual case and the no feedback case for $M1U2$ and $M2U1$ when removing the coupling is very little. We set the feedbacks a12 and a21 to be zero which are both key in coupling these two correlations and recalculated a11 and a22 (see Appendix). The correlations are slightly reduced from the actual to the no feedback uncoupled case in Fig. 17e at long lags, but the correlations at long lags in Fig. 17f are nearly identical to the correlations in the actual

case. As we did when comparing the no feedback case to the actual in the previous plot, we can also calculate the change in variance for the uncoupled case and compare that to the coupled case. We find that when we remove the coupling, the feedbacks account for less variance in EOF 1 and EOF2, at 33% and 46% respectively. This explains why we are seeing less change in the correlations between the no feedback and the actual case. Also, the feedback parameters (a11 = 0.0317 day^{-1} and a22 = 0.0556 day^{-1}, from Table 5) that we use when uncoupling the data are lower than the actual feedback parameters (a11 = 0.0545 day^{-1} and a22 = 0.0782 day^{-1}), from Table 4). The feedbacks are significantly lower when using the uncoupled method compared to the actual data. Also, the differences in the correlations between the no feedback case and the actual case for the uncoupled case are less than the changes in

	a11	**a12**	**a21**	**a22**
DJF Feedbacks Uncoupled	0.0189	0	0	-0.0304
MAM Feedbacks Uncoupled	-0.0159	0	0	0.0299
JJA Feedbacks Uncoupled	0.0317	0	0	0.0556
SON Feedbacks Uncoupled	0.0449	0	0	-0.0431

Table 5*. Feedback parameters for the Uncoupled case in* day^{-1}.

correlations for the actual data and the no feedback coupled case. It is important to use the two modes of variability and the coupling when trying to identify and quantify these feedbacks

between the eddy forcing and the zonal-mean zonal wind. Now that we have seen how the feedbacks and correlations change between the full data and the JJA, we can continue the analysis for the rest of the seasons.

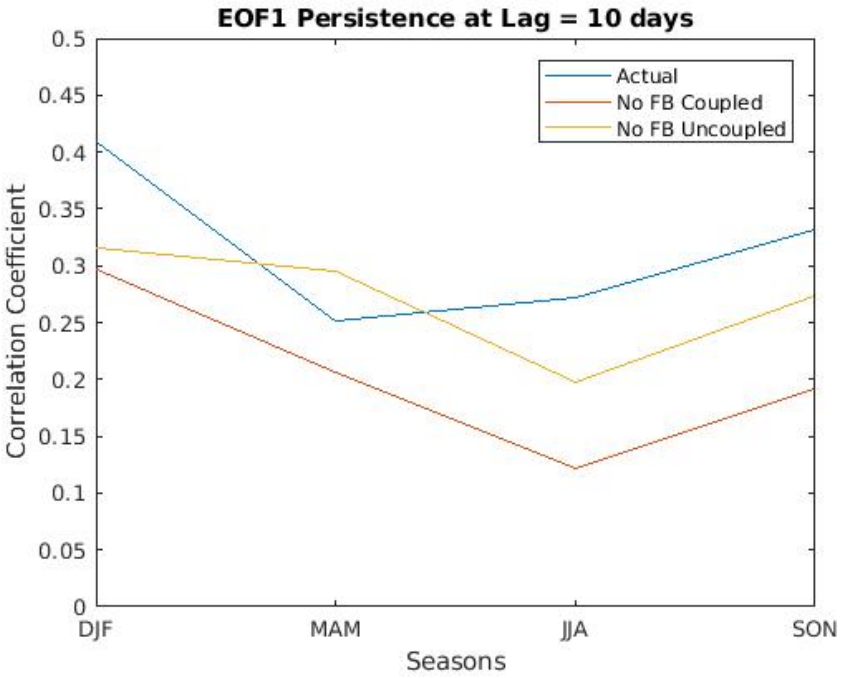

Figure 18. *EOF1 Persistence at lag = 10 days for all seasons for the a) actual coupled case (blue) b) the coupled no feedback case (red) and c) the uncoupled no feedback case.*

3.2.5.2 Seasonal Summary

In this section I will summarize some of the main points across the rest of the seasonal analysis. The correlation plots for the rest of the seasons can be found in the Appendix for those who want to look at each season more in-depth as we did for JJA. We will first look at the EOF1 of zonal wind persistence at lag = 10 days in Fig. 18. The reason we choose 10 days is because it is in the range of our longer lags that we have been investigating throughout this paper. We find that for EOF1, the persistence of zonal wind is lower in both the coupled and uncoupled no feedback cases except for the uncoupled MAM. This shows that there is an effect of these feedbacks on the persistence of the zonal wind. The feedbacks act to increase (decrease) the persistence of zonal wind if a11 and a22 are positive (negative) because as we saw in the synthetic data, the zonal wind now has an effect on the eddy momentum flux convergence. When there is no feedback presence, the eddy momentum flux convergence solely forces zonal wind and zonal wind does not force eddy

momentum flux convergence. For there to be a feedback, both must force each other and we see that to be the case in the actual data.

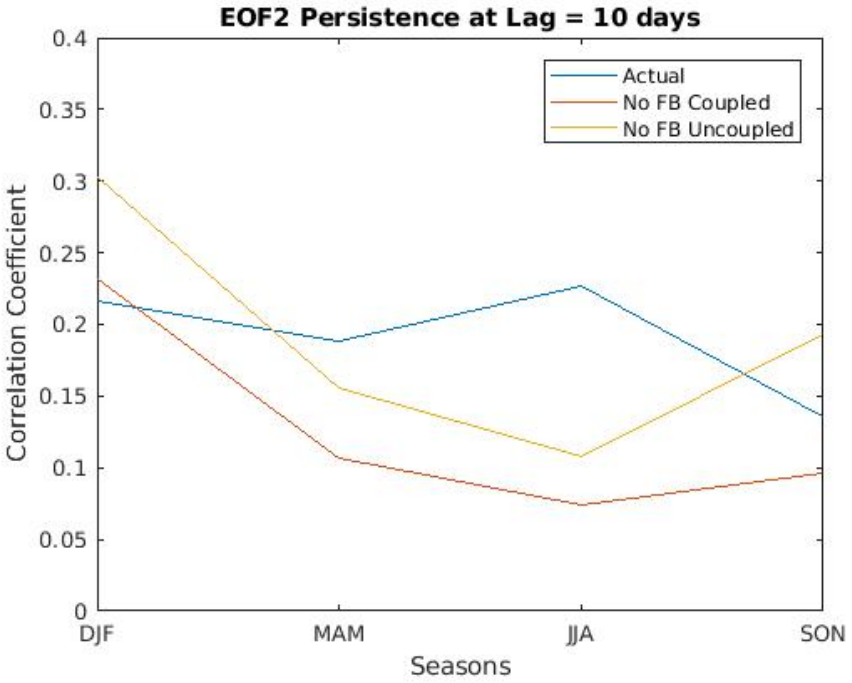

Figure 19. *EOF2 Persistence at lag = 10 days for all seasons for the a) actual coupled case (blue) b) the coupled no feedback case (red) and c) the uncoupled no feedback case.*

We see a similar tendency in Fig. 19 for EOF2 where the persistence in the no feedback cases is mostly reduced compared to the actual case. There are a couple of exceptions here in the uncoupled case (DJF, SON) and one in the coupled case (DJF) where the persistence actually increases when the feedbacks are removed. Again, we see these feedbacks having a significant impact on the zonal wind and they also play an important role on the change in variance which we will get to shortly.

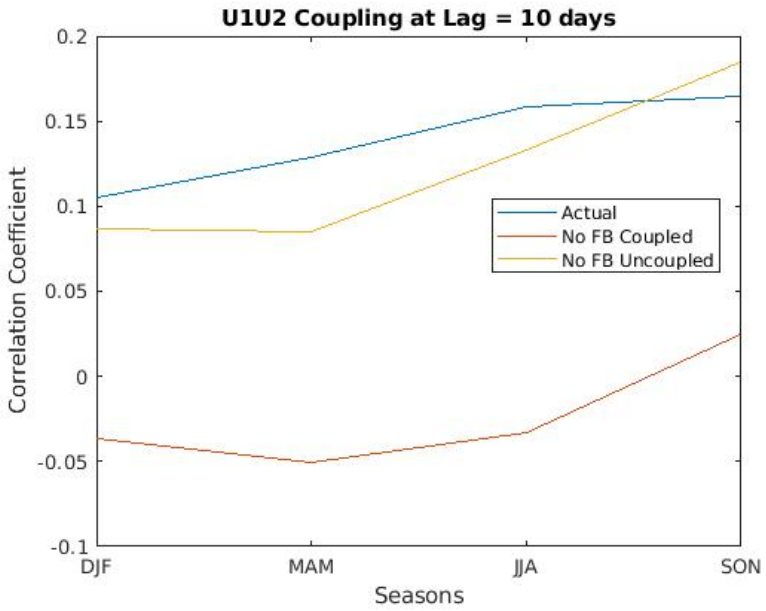

Figure 20. *U1 and U2 coupling at lag = 10 days for all seasons for the a) actual coupled case (blue) b) the coupled no feedback case (red) and c) the uncoupled no feedback case.*

In Fig. 20, we do the same thing for the $U1U2$ coupling. We see that with the exception of SON in the uncoupled case, removing the feedbacks reduces the correlations. We note again that $U1U2$ signifies the poleward propagation of the jet and so the positive correlations for the no feedback uncoupled are odd. The no feedback uncoupled case is almost unchanged from the actual case which shows that the coupling between modes must be assumed in order to account for the correlations between *U1* and *U2*. Because we can attribute some of the poleward propagation to the eddy-zonal flow feedbacks, we would not expect to see positive correlations for a no feedback case. Now there are some negative correlations for the coupled no feedback case, but they are much closer to zero as we would expect. We expect the positive correlations of $U1U2$ to be zero in the no feedback cases so when we see positive correlations for uncoupled case, it appears there is poleward propagation in the absence of feedbacks which is not expected and shows us that we should be using the coupling.

The final piece of analysis is the change of variance throughout the different seasons. We can see in Fig. 21 the different changes in variance for each mode across the seasons for both uncoupled and coupled.

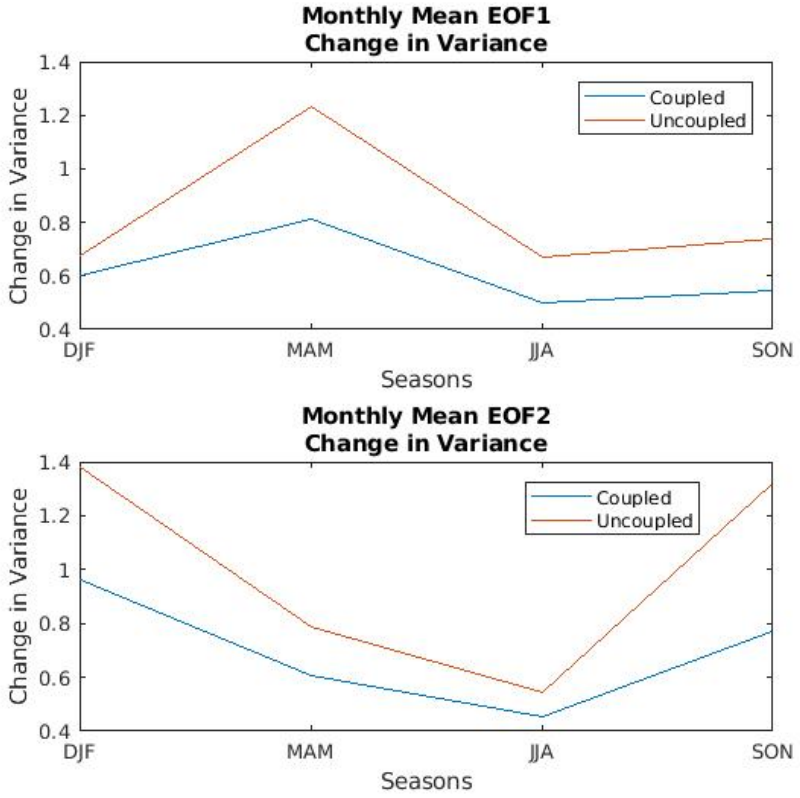

Figure 21. *Monthly mean change in variance for) EOF1 (top) and EOF2 (bottom) for both coupled (blue) and uncoupled case (red).*

We note that in EOF1, the change of variance for the coupled case ranges from about 0.5~0.8 which means that the feedbacks account for about 20%-50% of the variance. For EOF2, the coupled case changes of variance range from about 0.54~0.95 which means that the feedbacks account for about 4%-54% of the variance. This shows that the feedbacks account for a large amount of the zonal wind variability and varies across the different seasons. However, if we use the uncoupled feedbacks, we see that in DJF, JJA, and SON for EOF1 and MAM and JJA for EOF2, the feedbacks account for about 20%-40% of the variance. However, in the other seasons MAM for EOF1 and DJF and SON for EOF2, the feedbacks actually reduce the variance by 20%-40% which we would not expect and thus emphasizes that we need to use coupled feedbacks when analysis the eddy-zonal flow feedback effects on zonal wind variability.

4. Discussion

4.1 Quantifying Feedback Parameters

The first goal we achieved in this paper was quantifying the feedback parameters. We know that our technique for quantifying these parameters is accurate through the use of a synthetic dataset. We were able to reproduce the feedback parameters that we imposed onto the dataset. We knew exactly what the feedbacks were and found the feedbacks to be very close to the imposed feedbacks (see Table 2). We first found the feedback parameters for the entire ERA-Interim dataset in Table 3. We then divided the data into seasons to quantify the seasonal feedback parameters. It is useful to break the data down into seasons because there could be significant differences in the feedback parameters from season to season. We found that as expected, the feedback parameters did differ significantly throughout the seasons (see Table 4). The a11 feedback parameter was lowest in MAM and highest in JJA. Recall that a11 is the

feedback of PC1 on itself. The feedback parameter a12 was higher than a11 across all seasons. We found that the a21 feedback parameters was the only one that was negative. Recall that the a12 feedback is the effect of PC2 on PC1 and the a21 feedback is PC1 on PC2. The nature of opposite signs for a12 and a21 signify a poleward propagation of the zonal mean zonal wind due to the fact that a12 is positive meaning that when PC2 leads to PC1, the feedback is positive leads to a poleward shift. The a22 feedback parameter was lowest in DJF and highest in JJA. Recall that a22 is the feedback of PC2 on itself. Even though the feedback parameters seem small in magnitude, their impact can be large on the timescales involved in the annular modes.

4.2 Lagged Correlation Analysis

Through careful analysis of the lagged correlations, we were able to identify and visualize the feedbacks. We were able to identify feedbacks to varying extents throughout the different seasons. We see feedbacks in the form of non-zero correlations and we are focusing on the correlations at long positive lags because these lags are not affected by the obvious forcing of zonal wind by the eddies due to the momentum budget. In all seasons, we can identify positive correlations in the $M1U1$ plots, positive correlations in the $M1U2$ plots and negative correlations in the $M2U1$ plots at long positive lags. For $M2U2$, we see small but positive correlations at long positive lags in MAM and JJA. For DJF and SON, the correlations are much closer to zero and may be positive for a few time lags but are also slightly negative at some time lags. The positive correlations are much clearer in MAM and JJA for $M2U2$. We have identified the feedbacks present in these two modes of the zonal mean zonal wind and the eddy momentum fluxes.

When comparing the actual case compared to the feedbacks, we see some slight differences in the correlations as a result of the feedbacks being removed. In the correlations of $U1$, when the feedbacks are removed, the correlations drop below the actual case in all seasons except for MAM. For $U2$, the correlations when the feedbacks are removed are less than the actual case for all seasons except for SON where it looks like the no feedback case and the actual case are nearly identical. For $U1U2$, the correlations in the no feedback case quickly approach zero at long positive lags for MAM and JJA. In DJF, the correlations are slightly negative at long positive lags and for SON, the correlations are positive at long positive lags. For $M1U1$, the no feedback case has a slightly positive correlation for at long positive lags in MAM, JJA, and SON while DJF exhibits closer to zero correlation at these lags. The positive correlations at long positive lags shows the feedback that we are trying to identify. For $M2U2$, the no feedback slightly reduces the correlations at the long positive lags in all seasons except DJF where the no feedback case has nearly identical correlation values at long positive lags. For $M1U2$, the no feedback case reduces the correlations as expected for all seasons. For $M2U1$, the no feedback case increases (makes it less negative, even slightly positive) the correlations at long positive lags. It appears that the feedbacks present in these two cases ($M1U2$ and $M2U1$) likely signify poleward propagation because they are opposite in sign. The feedback parameters for a12 are positive and the feedback parameters for a21 are negative which bears this out. Removing the feedbacks, in most cases, does what we expect it to which is that it reduces the signal of a feedback in the correlations.

4.3 Change in Variance

Since we have two cases of our Reanalysis data (one as is and one with feedbacks removed), we can compare a quantify how much affect the feedbacks have on the total variability within each season (see Table 6). We see that in each season, the change in variance for 30-day running mean of EOF1 is less than 1 which means the removed feedbacks account for a certain percentage (between 20%-51%) of the total variance. In EOF 2, the change in variance for each season is less than 1 which means that the remove feedbacks account for a percentage of variance (4%-55%). The change of variance is important because we are looking to see what contribution the feedbacks have on the zonal-mean zonal wind and we find that the change in variance caused by feedbacks is rather large and at times, the feedbacks account for about half of the zonal wind variability.

	EOF1	EOF2
DJF	39% increase	4% increase
MAM	19% increase	40% increase
JJA	51% increase	55% increase
SON	45% increase	23% increase

Table 6*. Percent increase in the 30-day running mean variability attributed to feedback parameters for each season and each mode.*

4.4 Coupled vs. Uncoupled

One of the main focuses of this study was to emphasize the importance of using multiple modes of variability to solve for the feedbacks. We mentioned earlier than past studies focused heavily on just the leading mode of variability and do not account for the coupling potential between modes. Once we completed the analysis for our seasonal ERA-Interim data, we quickly

replicated the process to attempt to illustrate the uncoupled results for the same dataset. We simplified the feedback calculation and set the coupling feedbacks (a12 and a21) to zero so that the feedbacks would change slightly and become uncoupled. We found that for nearly all seasons, the uncoupled case very closely represented the actual data. While there were some subtle differences in magnitude for the no feedback uncoupled case, the general shapes of the correlation plots were similar. Because the no feedback case here is so close to the actual case, we can infer that the uncoupled case is not able to accurately depict the effects of the feedbacks. We note that the uncoupled feedback parameters (a11 and a22) also vary in sign from season to season much more than the coupled case where the signs for all feedbacks were consistent between the different seasons. For EOF 1 for MAM and EOF 2 for DJF and SON, the change of variance is greater than 1 which means that the presence of feedbacks actually serves to reduce the variability which does not make much physical sense. We expect that feedbacks will account for a portion of the zonal wind variability which is the case in both modes for the coupled case. It is important to make sure that when we are solving for the feedbacks, we are using a coupled two-mode feedback method to more accurately depict the effects of the feedbacks on the zonal-mean zonal wind.

4.5 Future Research

The scope of this analysis allows for some potential areas of future research that could provide for a nice continuation of this analysis. First off, this analysis was limited to the Southern Hemisphere. The analysis could be extended to the Northern Hemisphere as well. Investigating the Northern Hemisphere would allow for a comparison between the two hemispheres to see how the feedbacks affect the jets in each hemisphere differently. Another

clear path for future research would be to investigate what is happening at short lags. We only focused on the longer-term feedbacks that we see in the lagged correlation analysis.

5. Conclusions

In this study, we have presented an analysis of the role of eddy-zonal flow feedback on the zonal wind variability through two modes of variability using primarily ERA-Interim reanalysis data. We used a synthetic dataset as a proof of concept of how to accurately back out the different feedback parameters. Once we knew that we could back out the feedback parameters, we moved on to ERA-Interim reanalysis and followed the same steps to assess the main objectives of this research. We found that we were able to identify the seasonal feedback parameters using a two-mode approach. We utilized lagged correlation analysis to visually identify and represent the feedbacks between the different modes of the zonal-mean zonal wind and the eddy momentum flux convergence. Then, we were able to quantify the seasonal feedback parameters using the covariances at time lag = 0. It is imperative to perform the analysis seasonally because there is significant change in the feedback parameters from season to season. Without doing so, the results for the feedback parameters may not give the most accurate depiction of the eddy-zonal flow feedback. Our last step involved taking the feedback parameters and creating a dataset that removes the feedbacks to see how much impact the feedbacks have on the variability. With inaccurate feedback parameters, we could not perform this crucial step. We found that the feedbacks significantly affect the variability of the zonal wind. The feedbacks mostly act to increase variability in EOF 1 but they act to reduce the variability in EOF 2. The last step we took was to investigate the importance of the coupled vs. uncoupled feedbacks. We found that the uncoupled case does not account for the feedbacks

nearly as well as the coupled case which leads to large variability in the change of variance values.

In summary, we were able to first emphasize the importance of using coupled instead of uncoupled feedbacks. We then identified feedbacks using lagged correlation analysis. Next, we quantified the feedback parameters across both modes of variability. And finally, we assessed the impact of feedbacks on the zonal wind variability. We found that using coupled feedbacks is crucial to understand the full effects of the eddy-zonal flow feedbacks. The feedbacks can have such a large impact on the zonal wind variability, where at times, the feedbacks increase variability by greater than 50% for the change of variance of the 30-day running mean. We utilized the first two dominant modes of variability to better understanding of the eddy-zonal flow feedbacks and their effect on the zonal wind variability.

6. Appendix

6.1 Principal Components → Power Spectra → Covariance → Correlation

To go from Principal Components to correlation via Fourier transforms necessitates some careful mathematics to make sure we are not losing any important information. Earlier in the paper, we referenced that once we get the principal components, we can easily convert to correlations but there are a few steps in between principal components and correlation.

Once we have the principal components, we need to convert the principal components to power spectra. With power spectra in hand, we set up a function of our own that converts to covariances. We utilize a Fourier series to do this conversion. It is a fairly complex step, but the important thing to remember is that through the Fourier series, all of the necessary information is conserved.

Once we have the covariances calculated, we simple convert them into correlations by dividing the covariance by the square root of the covariance at lag = 0. Two examples of the equation are shown below:

$$corr\ U1 = \frac{cov(U1)}{cov(U1)@\ lag{=}0} \qquad \textbf{Equation 26}$$

$$corr\ U1U2 = \frac{cov(U1U2)}{\sqrt{cov(U1)@\ lag{=}0}\sqrt{cov(U2)@\ lag{=}0}} \qquad \textbf{Equation 27}$$

6.2 Backing out Tau

In the ERA-Interim reanalysis, we were also able to back out the τ, which is the damping timescale. Just like the we did with the feedback parameters, we used the synthetic dataset to show that we could accurately back out τ when we imposed τ = 8 days. In the synthetic dataset,

we only used one τ, but we could have used two different τ as τ is slightly different between the two modes. The equations we used were:

$$\tau_{1=} \frac{cov(M1U1)}{cov(U1)} \quad \textbf{Equation 28}$$

$$\tau_{2=} \frac{cov(M2U2)}{cov(U2)} \quad \textbf{Equation 29}$$

Table 5 shows the results for the backed-out τ values. Table 6 also shows the τ values for the no feedback cases as well. We can solve the no feedback case the same way using earlier equations, except we just use the no feedback corresponding covariances.

	τ_1	τ_2	τ_1 No Feedback	τ_2 No Feedback
Full ERA-Interim	7.1371	6.9506	7.2739	7.1101
DJF	9.3130	9.4314	8.54	8.0529
MAM	7.1562	7.0686	6.5429	6.1555
JJA	6.1402	6.0773	5.3881	5.1929
SON	6.8844	6.8778	6.3132	5.8758

Table 7. *Backed out τ values for EOF1 and EOF2 for ERA-Interim Seasonal data and the no feedback case*

6.3 Initial Coupled → Uncoupled

To create an uncoupled version of the data to compare with our original results, we had to change slightly how we calculated the feedbacks. Eqs. 11 and 12 show the complex matrix equation that we needed to use to solve for each of the 4 feedback parameters. However, by uncoupling the feedbacks, we change our way of calculating the feedbacks and set the coupled feedbacks (a12 and a21) to zero.

$$\dot{a11} = \frac{cov(M1U1)}{cov(U1)} \quad \textbf{Equation 30}$$

$$\dot{a22} = \frac{cov(M2U2)}{cov(U2)} \quad \textbf{Equation 31}$$

Where the dot simply denotes that these are the uncoupled feedback parameters.

6.4 More Seasonal Correlation Plots

This section will include the rest of the seasonal correlations plots that we did not discuss in detail within the paper. In the paper, we discussed in great detail JJA, and summarized the rest, but here we will show DJF, MAM, and SON for completeness. In each of these figures, the plots show three different cases: the actual coupled case (blue), the no feedback coupled case (red) and the no feedback uncoupled case (yellow).

Figure 22 shows the cross correlations for December-January-February (DJF) which is the Southern Hemisphere summer.

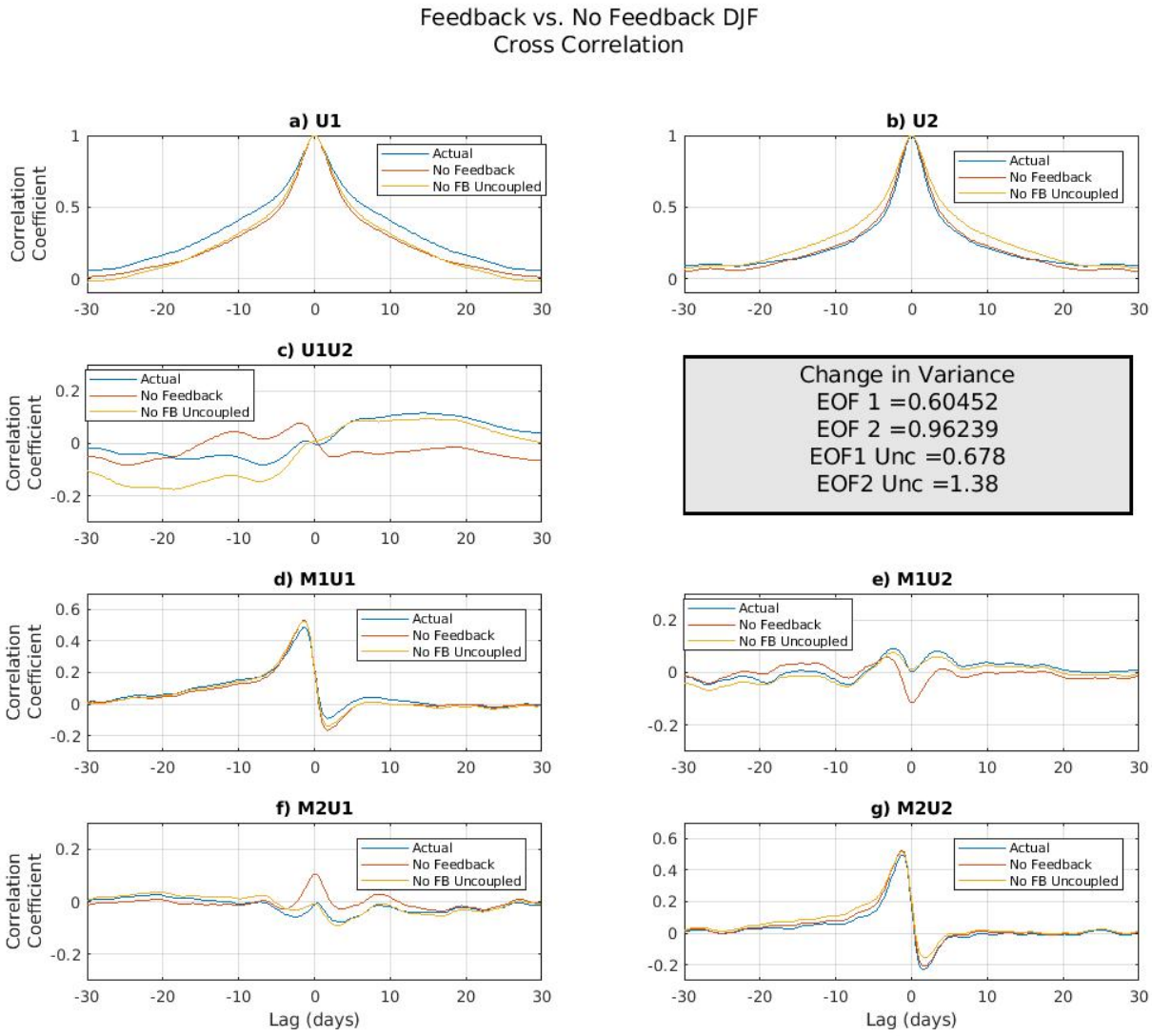

Figure 22. *DJF Lagged Correlation analysis for actual coupled (blue), coupled no feedback case (red) and uncoupled no feedback case (yellow). A) Auto correlation of U1 B) Auto correlation of U2 C) Cross correlation of U1U2 D) Cross Correlation of M1U1 E) Cross correlation of M1U2 F) Cross correlation of M2U1 G) Cross Correlation of M2U2.Change of Variance also shown for both modes.*

Figure 23 shows the cross correlations for March-April-May (MAM).

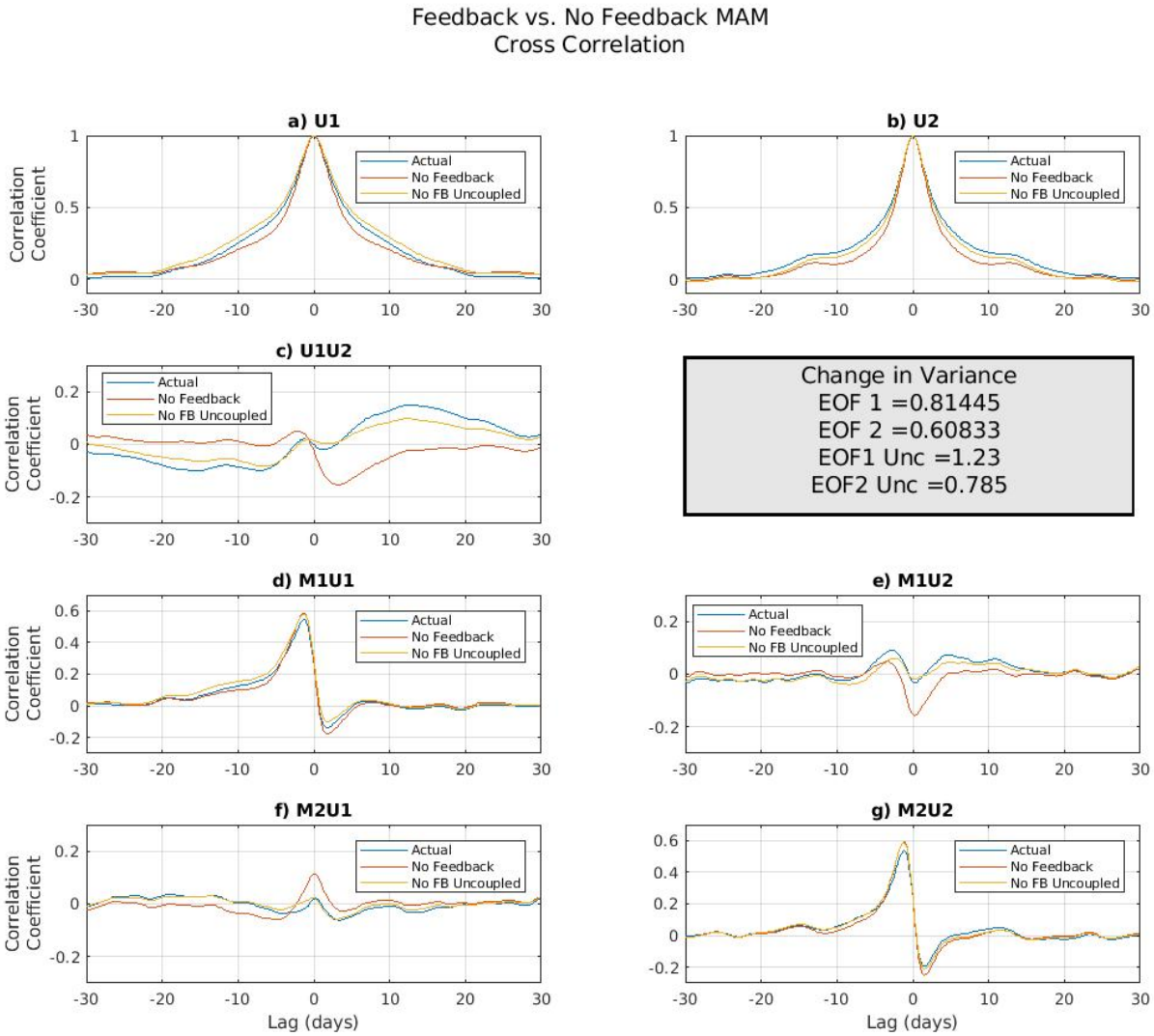

Figure 23. *MAM Lagged Correlation analysis for actual coupled (blue), coupled no feedback case (red) and uncoupled no feedback case (yellow). A) Auto correlation of U1 B) Auto correlation of U2 C) Cross correlation of U1U2 D) Cross Correlation of M1U1 E) Cross correlation of M1U2 F) Cross correlation of M2U1 G) Cross Correlation of M2U2.Change of Variance also shown for both modes.*

Figure 24 shows the cross correlations for September-October-November (SON).

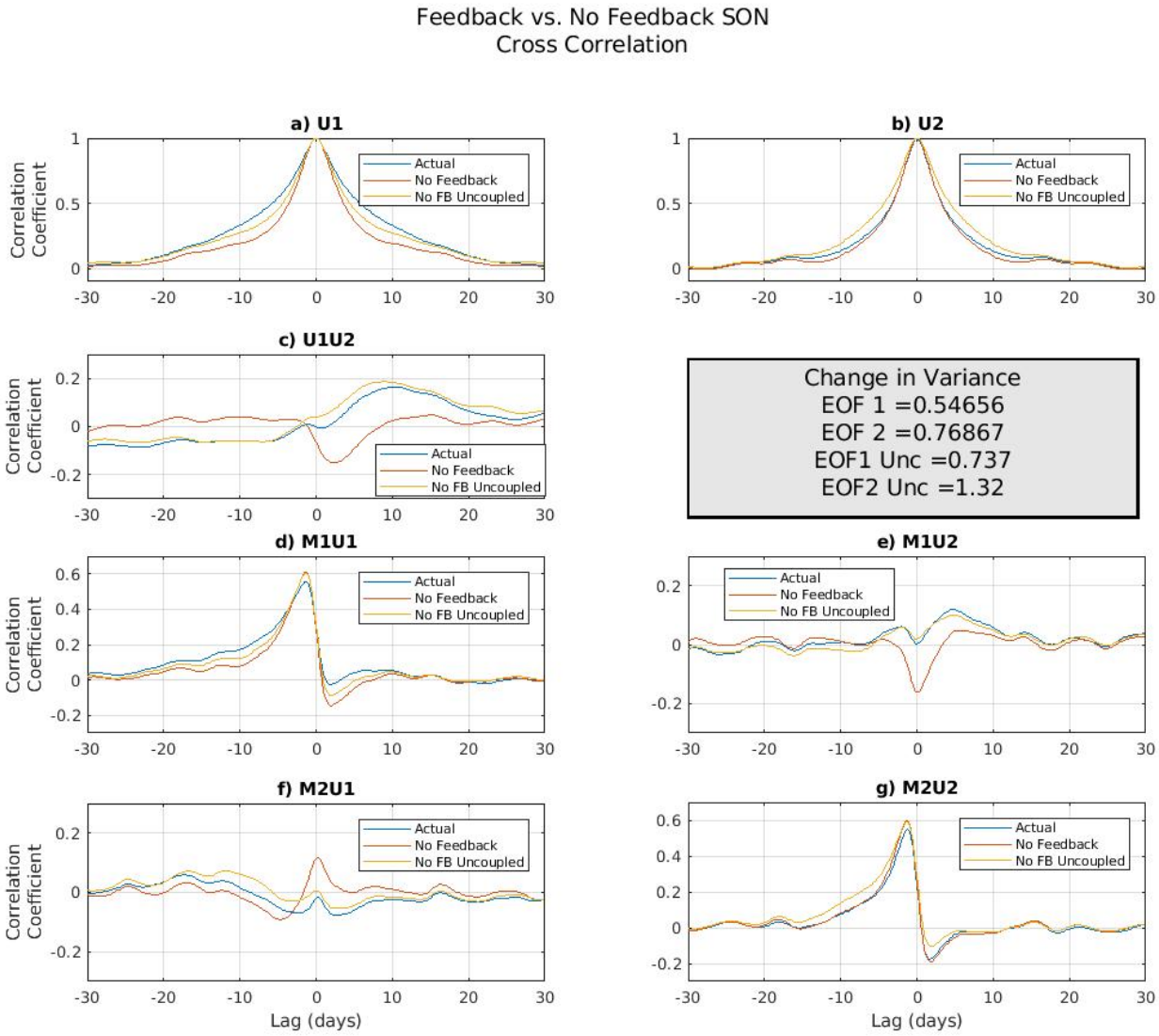

Figure 24. *SON Lagged Correlation analysis for actual coupled (blue), coupled no feedback case (red) and uncoupled no feedback case (yellow). A) Auto correlation of U1 B) Auto correlation of U2 C) Cross correlation of U1U2 D) Cross Correlation of M1U1 E) Cross correlation of M1U2 F) Cross correlation of M2U1 G) Cross Correlation of M2U2.Change of Variance also shown for both modes.*

7. References

Barnes , E. A., & Polvani , L. (2013). Response of the midlatitude jets, and of their variability, to increased greenhouse gases in the CMIP5 Models. *Journal of Climate, 26*, 7117-7135.

Byrne, N. J., Shepherd, T. G., Woolings, T., & Plumb, R. (2016). Annular modes and apparent eddy feedbacks in the southern hemisphere. *Geophysical Research Letters, 43*, 3897-3902.

Codron, F. (2004). Relation Between Annular Modes and the Mean State: Southern Hemispher Summer. *Journal of Climate, 18*, 320-340.

Dee, D., Uppala, S., Simmons, A., Berrisford, P., Poli, P., Kobayashi, S., . . . Beljaars, A. (2011). The ERA-Interim reanalysis: configuration and performance of the data assimilation system. *Quarterly Journal of the Royal Meteorological Society, 137*, 553-597.

Eichelberger, S. J., & Hartmann, D. L. (2007). Zonal Jet Structure and the Leading Mode of Variability. *Journal of Cliamte, 20*, 5149-5163.

Feldstein, S. B. (1998). An observational study of the intraseasonal poleward propagation of zonal mean flow anomalies. *Journal of the Atmospheric Sciences, 55*, 2516-2529.

Feldstein, S., & Lee, S. (1998). Is the atmospheric zonal index driven by an eddy feedback? *Journal of Atmospheric Sciences, 55*, 3077-3086.

Gerber, E. P., & Vallis, G. K. (2006). Eddy-Zonal Flow Interactions and the Persistence of the Zonal Index. *Journal of Atmospheric Sciences, 64*, 3296-3311.

Gillett, N. P., Kell, T. D., & Jones, P. D. (2006). Regional climate impacts of the southern annular mode. *Geophysical Research Letters, 33*, L23704.

Hannachi, A., Jolliffe, I. T., & Stephenson, D. B. (2007). Empirical orthogonal functions and related techniques in atmospheric science: A Review. *International Journal of Climatology, 27*, 1119-1152.

Hartmann, D. L., & Lo, F. (1998). Wave-driven zonal flow vascillation in the Southern Hemisphere. *Journal of Atmospheric Sciences, 55*, 1303-1315.

Kidston, J., & Gerber, E. P. (2010). Intermodal variability of the poleward shift of the austral jet stream in the CMIP3 integrations linked to biases in 20th century climatology. *Geophysical Research letters, 37*, L09708.

Kidston, J., Frierson, D. W., Renwick, J. A., & Vallis, G. K. (2010). Observations, simulations, and dynamics of jet stream variability and annular modes. *Journal of Climate, 23*, 6186-6199.

Kisdon, J. W. (1988). Indices of the Southern Hemispher zonal wind. *Journal of Climate, 1*, 183-194.

Kuroda, Y., & Mukougawa, H. (2011). Role of medium-scale waves on southern annular mode. *Journal of Geophysical Research, 116*, D22107.

Lorenz, D. (2014). Understanding midlatitude jet variability and change using rossby wave chromatography: poleward-shifted jets in response to external forcing. *Journal of Atmospheric Sciences, 71*, 2370-2389.

Lorenz, D. (2015). Understanding midlatitude jet variability and change using rossby wave chromatography: methodology. *Journal of the Atmospheric Sciences, 72*, 369-388.

Lorenz, D. J., & Hartmann, D. L. (2001). Eddy-zonal flow feedback in the southern hemisphere. *Journal of Atmospheric Sciences, 58*, 3312-3327.

Lorenz, D. J., & Hartmann, D. L. (2003). Eddy-zonal flow feedback in the northern hemisphere winter. *Journal of Climate, 16*, 1212-1227.

Ma, D., Hassanzadeh, P., & Kuang, Z. (2017). Quantifying the eddy-jet feedback strength of the annular mode in an idealized GCM and reanalysis data. *Journal of the Atmospheric Sciences, 74*, 393-407.

Monahan, A. H., Fyfe, J. C., Ambaum, M. H., Stephenson, D. B., & North, G. R. (2009). Empirical orthogonal functions: the medium is the message. *Journal of Climate, 22*, 6501-6514.

Namias, J. (1950). The index cycle and its role in the general circulation. *Journal of Meteorology, 7*, 130-139.

Nigam, S. (1990). On the structure of the observed tropospheric and stratospheric zonal-mean wind. *Journal of Atmospheric Science, 47*, 1799-1813.

Panetta, R. L. (1992). Zonal jets in wide baroclinically unstable regions: persistence and scale selection. *Journal of Atmospheric Sciences, 50*, 2073-2106.

Riviere, G. (2011). A dynamical interpretation of the poleward shift of the jet streams in global warming scenarios. *Journal of Atmospheric Sciences, 68*, 1253-1272.

Riviere, G., Robert, L., & Codron, F. (2016). A short-term negative eddy feedback on midlatitude jet variability due to planetary wave reflection. *Journal of the Atmospheric Sciences, 73*, 4311-4328.

Robinson, W. A. (1994). Eddy feedbacks on the zonal index and the eddy-zonal flow interactions induced by zonal flow transience. *Journal of Atmospheric Science, 51*, 2553-2562.

Robinson, W. A. (2016). The dynamics of the zonal index in a simple model of the atmosphere. *Tellus A: Dynamic Meteorology and Oceanography, 43A*, 295-305.

Rossby, C. G. (1939). Relations between variations in the intensity of the zonal circulation and the displacements of the semi-permanent centers of action. *Journal of Marine Research, 2*, 38-55.

Simpson, I. R., Shaw, T. A., & Seager, R. (2014). A diagnosis of the seasonally and longitudinally varying midlatitude circulation response to global warming. *Journal of Atmospheric Science, 71*, 2489-2515.

Simpson, I. R., Shepherd, T. G., Hitchcock, P., & John, S. F. (2013). Southern annular mode dynamics in O=observations and models. Part II: Eddy feedbacks. *Journal of Climate, 26*, 5220-5241.

Son, S.-W., & Lee, S. (2006). Preferred modes of variability and their relationship with climate change. *Journal of Climate, 19*, 2063-2075.

Thompson, D. W., & Wallace, J. M. (2000). Annular modes in the extratopical circulation. Part II: trends. *Journal of Climate, 13*, 1018-1036.

Thompson, D. W., & Wallace, J. M. (2000). Annular modes in the extratropical circulation. Part 1: month-to-month variability. *Journal of Climate, 13*, 1000-1016.

Weare, B. C., & Nasstrom, J. S. (1982). Exampled of extended empirical orthogonal function analyses. *Monthly Weather Review, 110*, 481-485.

Willett, H. C. (1948). Long-period fluctuations of the general circulation of the atmosphere. *Journal of Meteorology, 6*, 34-50.

Yin, J. H. (2005). A consistent shift of the storm tracks in simulations of the 21st century climate. *Geophysical Research Letters, 32*, L18701.